

---

# GEDAN: Learning the Edit Costs for Graph Edit Distance

---

**Francesco Leonardi**  
Institute of Computer Science  
University of Bern  
Neubrückestrasse 10, 3012 Bern, Switzerland  
francesco.leonardi@unibe.ch

**Markus Orsi**  
Department of Chemistry  
University of Bern  
Freiestrasse 3, 3012 Bern, Switzerland  
markus.orsi@unibe.ch

**Jean-Louis Reymond**  
Department of Chemistry  
University of Bern  
Freiestrasse 3, 3012 Bern, Switzerland  
jean-louis.reymond@unibe.ch

**Kaspar Riesen**  
Institute of Computer Science  
University of Bern  
Neubrückestrasse 10, 3012 Bern, Switzerland  
kaspar.riesen@unibe.ch

## Abstract

Graph Edit Distance (GED) is defined as the minimum cost transformation of one graph into another and is a widely adopted metric for measuring the dissimilarity between graphs. The major problem of GED is that its computation is NP-hard, which has in turn led to the development of various approximation methods, including approaches based on neural networks (NN). Most of these NN-based models simplify the problem of GED by assuming unit-cost edit operations—a rather unrealistic constraint in real-world applications. In this work, we present a novel Graph Neural Network framework that approximates GED using both supervised and unsupervised training. In the unsupervised setting, it employs a gradient-only self-organizing mechanism that enables optimization without ground-truth distances. Moreover, a core component of our architecture is the integration of a Generalized Additive Model, which allows the flexible and interpretable learning of context-aware edit costs. Experimental results show that the proposed method achieves similar results as state-of-the-art reference methods, yet significantly improves both adaptability and interpretability. That is, the learned cost function offers insights into complex graph structures, making it particularly valuable in domains such as molecular analysis and structural pattern discovery.

## 1 Introduction and Related Work

Graphs are a versatile data structure that can be used to represent both the features of entities and the relationships between them. Due to their power and flexibility, graphs have found numerous applications. For example, graph-based representations are successfully used in the analysis of social networks [1], the recognition of human poses [2], the modeling of road infrastructure [3] or the representation of watercourses [4]. Graphs can also be used in bio-informatics and computational chemistry, for example, to represent proteins [5] or molecules [6], the field we consider as possible application in this paper.

In the last decades, several methods have been proposed and researched to assess the dissimilarity or similarity between graphs, such as diverse graph kernels or graph matching procedures [7]. Among these, *Graph Edit Distance* (GED) [8] can be interpreted as a standard approach. Basically, GED measures the distance between two graphs in terms of the minimum cost operations required to

transform one graph into the other. The considered operations typically include insertions, deletions and substitutions of both nodes and edges. One of the most important advantages of GED is that it can be applied to virtually all types of graphs and thus, GED can be flexibly adapted to any graph-based application. However, exact computation of GED is an NP-hard problem [9], which makes its application to larger graphs, or in scenarios requiring a large number of comparisons, impractical.

To address this limitation and to reduce the computational complexity of GED, several strategies for relaxing the problem have been proposed. These techniques range from binary linear programming [10], over fast suboptimal algorithms preserving classification accuracy [11, 12], to quadratic assignment models [13] and local search algorithms [14]. More recently, diverse approaches to learn and approximate GED using *Graph Neural Networks* (GNNs) have been proposed [15–17]. A very recent approach [18], also based on GNNs, differs from the others in explicitly formulating the GED as a matrix optimization problem. That is, this method approximates the GED by learning the permutation that minimizes the assignment cost between the substructures of two graphs.

Since the GNN-based methods for learning GED are trained in a supervised manner, a ground truth is required for the distances between the training graphs. Clearly, this is a significant limitation as the computation of the actual distances between graphs stemming from large datasets is computationally prohibitive, limiting the practical applicability of these methods. This contradiction was recently pointed out by Yang et al. [19], who proposed strategies such as transfer learning and few-shot learning to mitigate the problem.

A second problem is that the vast majority of the GNN-based approaches assume unit costs for the individual operations. This can be regarded as particularly restrictive in graph-based applications in chemistry or bio-informatics, where nodes and edges of graphs are often used to represent atoms and chemical bonds, respectively. In this context, it is known that the substitution of atoms, or functional groups, does not occur at uniform cost, but depends on specific structural and functional factors [20, 21].

Our paper addresses the two challenges mentioned above separately. First, based on the idea proposed by Jain et al. [18], our novel model combines GNNs [22] with *Generalized Additive Models* (GAMs) [23] and approximates the GED by a soft-assignment obtained with a Gumbel-Sinkhorn network [24]. A key advantage of this novel approach is that it can be used in unsupervised contexts, eliminating the need for explicit ground truth distances. Second, unlike previous methods, our approach learns edit costs directly through gradient descent, making the GED consistent with respect to graph properties. The benefit of this approach is that the learned costs might reveal lesser-known relationships between the underlying graphs and provide new insights for domain experts.

The remaining paper is structured as follows. In Section 2, we describe both the method used to approximate the GED and the method to learn the costs of the edit operations. In Section 3, we present the results of our experimental evaluation and present a use case of our novel approach stemming from the field of computational chemistry. In Section 4, we conclude the paper and propose future research work directions.

## 2 Methods

In the present paper, we define a graph as a triple  $G = (V, E, \mu)$ , where  $V$  is the set of nodes,  $E \subseteq \{(u, v) | u, v \in V, u \neq v\}$  is the set of edges, and  $\mu : V \rightarrow L$  is a function that assigns a label  $\mu(v) = l \in L$  to each node  $v \in V$  (where  $L$  is a given label alphabet). Sometimes this definition is complemented with a second function, which also assigns a label to the edges in the graph. In this paper, however, we only use node-labeled graphs (in fact, the methods proposed in this section could also be adapted to labeled edges).

The overall aim of our novel method is to compute the Graph Edit Distance  $\text{GED}(G, G')$  between two graphs  $G$  and  $G'$ . Our approach is based on a reformulation of the problem of GED to a *Quadratic Assignment Problem* (QAP) [13] as proposed in [18]. However, the method proposed in this paper (illustrated in Fig. 1) differs significantly from the previous approaches in four key aspects, which are discussed in detail in the following four subsections.

1. By adopting the message passing mechanism of GNNs, we introduce a system of additive penalties for dissimilar node representations. This means that we not only consider the nodes and their representations, but also take their growing neighboring structures into account.

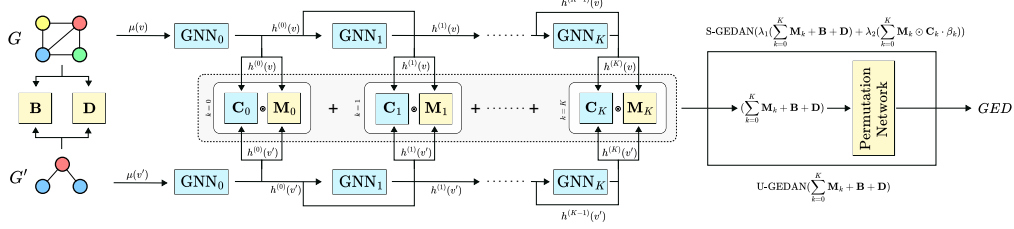


Figure 1: Structure of the GEDAN architecture. Learnable layers are shown in blue color, static or frozen layers are shown in yellow color.

2. Instead of learning the optimal permutation for the underlying QAP directly, we use a Gumbel-Sinkhorn network in a pre-trained way to approximate a *Linear Sum Assignment Problem* (LSAP). Moreover, we define the framework so that it allows for unsupervised training, which enhances its practical applicability.
3. Our method learns the edit costs for nodes and edges and, to enable greater flexibility, we generalize these scalar costs to node-dependent cost matrices, which are learned via an auxiliary neural network.
4. The new formulation allows the model to assign context-aware, node-specific edit costs during training, exploiting a double loss deployed in other metric learning frameworks.

## 2.1 Penalization with Message Passing

Let  $G = (V, E, \mu)$  and  $G' = (V', E', \mu')$  be two graphs with  $n$  and  $m$  nodes, respectively. To make  $G$  and  $G'$  of equal size, we pad them with  $|V'|$  and  $|V|$  dummy nodes termed  $\epsilon$ , which are all assigned a special label  $\mu(\epsilon)$ . Let  $\tilde{V} = V \cup \{\epsilon\}_{|V'|}$  and  $\tilde{V}' = V' \cup \{\epsilon\}_{|V|}$  be the sets of nodes of the padded graphs, for any node  $v \in \tilde{V}$  (or  $v' \in \tilde{V}'$ ), we define the  $k$ -th level representation as

$$h^{(k)}(v) = \begin{cases} \mu(v), & \text{if } k = 0, \\ A^k (h^{(k-1)}(v)) + h^{(k-1)}(v), & \text{if } k > 0, \end{cases} \quad (1)$$

where  $A^k$  is an injective neighborhood aggregation function that captures information up to the  $k$ -hop neighborhood of node  $v$ , while preserving its structural uniqueness. In our implementation, we instantiate  $A^k$  as the *Graph Isomorphism Network* (GIN) [25], which generalizes the *Weisfeiler-Lehman* test [26] and is known for its expressive power in distinguishing graph structures.

Next, we define  $d^{(k)} : \tilde{V} \times \tilde{V}' \rightarrow \mathbb{R}_{\geq 0}$  as a distance function between  $d$ -dimensional node embeddings  $h^{(k)}(v)$  and  $h^{(k)}(v')$  at level  $k$  by means of the normalized cosine dissimilarity

$$d^{(k)}(v, v') = \frac{1}{2} \left( 1 - \frac{\langle h^{(k)}(v), h^{(k)}(v') \rangle}{\|h^{(k)}(v)\| \cdot \|h^{(k)}(v')\|} \right). \quad (2)$$

A distance  $d^k(v, v')$  of 0 indicates identical representations  $h^{(k)}(v)$  and  $h^{(k)}(v')$ , and values close to 1 indicate a high dissimilarity between these representations. We define the multi-scale distance  $d^K(v, v')$  between nodes  $v \in \tilde{V}$  and  $v' \in \tilde{V}'$  as

$$d^K(v, v') = \sum_{k=0}^K d^{(k)}(v, v'). \quad (3)$$

This formulation enables a hierarchical comparison of nodes, where each term  $d^{(k)}(v, v')$  evaluates the dissimilarity based on neighborhood information of  $v$  and  $v'$  of increasing radius. The resulting distance  $d^K(v, v')$  is zero if, and only if, both nodes and their surrounding structures are equal.

**Identity condition.** The function  $d^K(v, v')$  satisfies the following identity property:

$$d^K(v, v') = 0 \iff \text{sub}^{(K)}(G, v) \cong \text{sub}^{(K)}(G', v'), \quad (4)$$

where  $\text{sub}^{(K)}(G, v)$  is the  $K$ -hop neighborhood graph anchored at node  $v \in \tilde{V}$  which contains all nodes that have shortest path length at most  $K$  to node  $v$ , and  $\cong$  indicates that there exists a label-preserving graph isomorphism.

### Proof Sketch

- **Case 1:** If  $\mu(v) \neq \mu'(v')$ , then  $h^{(0)}(v) \neq h^{(0)}(v')$ , and hence  $d^{(0)}(v, v') > 0$ , which implies  $d^K(v, v') > 0$ .
- **Case 2:** If  $\mu(v) = \mu'(v')$  but  $\text{sub}^{(K)}(G, v) \not\cong \text{sub}^{(K)}(G', v')$ , the injectivity of  $A^k$  ensures that structural differences will be reflected in the representations at some  $k \leq K$ . To prevent over-smoothing, where embeddings become indistinguishable as  $k$  increases, we use residual connections in Eq. 1. As demonstrated in [27], this strategy preserves discriminative power across layers. Therefore, there will exist at least one  $k$  such that  $h^{(k)}(v) \neq h^{(k)}(v')$ , implying  $d^K(v, v') > 0$ .

## 2.2 U-GEDAN Model

For our novel model we first construct a series of  $[n + m] \times [m + n]$  distance matrices  $\mathbf{M}_k = (m_{ij})_{[n+m] \times [m+n]}$ , where element  $m_{ij}$  encodes the dissimilarity  $d^{(k)}(v_i, v_j)$  between the  $i$ -th node of  $G$  and the  $j$ -th node of  $G'$  at level  $k$  (see Eq. 2). Formally, we use the following structure

$$\mathbf{M}_k = \left[ \begin{array}{ccc|cc} d^{(k)}(v_0, v'_0) & \dots & d^{(k)}(v_0, v'_m) & d^{(k)}(v_0, \epsilon) & \infty \\ \vdots & \ddots & \vdots & & \ddots \\ d^{(k)}(v_n, v'_0) & \dots & d^{(k)}(v_n, v'_m) & \infty & d^{(k)}(v_n, \epsilon) \\ \hline d^{(k)}(\epsilon, v'_0) & & \infty & & \\ & \ddots & & & \\ \infty & & d^{(k)}(\epsilon, v'_m) & & 0 \end{array} \right]. \quad (5)$$

To combine the  $(K + 1)$  multi-scale matrices  $\mathbf{M}_0, \dots, \mathbf{M}_K$ , we employ the *Generalized Additive Model* (GAM) framework [23], recently shown to enhance interpretability in deep models [28]. Next, we define a cost matrix  $\mathbf{D} = (d_{ij})_{[n+m] \times [m+n]}$  with

$$d_{ij} = \text{ReLU}(\deg(v_i) - \deg(v'_j)) \cdot b^\ominus + \text{ReLU}(\deg(v'_j) - \deg(v_i)) \cdot b^\oplus, \quad (6)$$

where  $\deg(v)$  denotes the degree of node  $v$  and  $b^\ominus$  and  $b^\oplus$  correspond to the cost of edge deletions and insertions, respectively. Matrix  $\mathbf{D}$  therefore stores the costs of the edge operations, which are implied by the corresponding node operations (assuming unlabeled edges).

Similarly, we construct a second base cost matrix  $\mathbf{B} = (b_{ij})_{[n+m] \times [m+n]}$  with

$$b_{ij} = \begin{cases} a^\ominus, & \text{if } i < n \text{ and } j \geq m, \\ a^\oplus, & \text{if } i > n \text{ and } j \leq m, \\ 0 & \text{else,} \end{cases} \quad (7)$$

where  $a^\oplus$  and  $a^\ominus$  correspond to the cost of node insertions and deletions respectively. Hence, matrix  $\mathbf{B}$  encodes the costs of node deletions and insertions in the lower-left and upper-right corners of the matrix, respectively, while all other entries are set to zero. Combining matrices  $\mathbf{M}$ ,  $\mathbf{D}$ , and  $\mathbf{B}$  aligns conceptually with the reformulation of the GED problem as an LSAP [12]. In our formulation, however, insertions and deletions are not restricted to diagonal elements but we implement a masking mechanism that hides off-diagonal entries from the network, ensuring they do not influence the learning process.

Finally, using a pre-trained Gumbel-Sinkhorn network [24], we calculate a soft permutation matrix  $\mathbf{P}$  on  $\sum_{k=0}^K \mathbf{M}_k + \mathbf{B} + \mathbf{D}$ . Formally,

$$\mathbf{P} = \text{Gumbel-Sinkhorn} \left( \sum_{k=0}^K \mathbf{M}_k + \mathbf{B} + \mathbf{D} \right). \quad (8)$$

By multiplying the resulting soft permutation matrix  $\mathbf{P}$  element-wise with the argument of Eq. 8, we obtain our first approximation of the GED

$$\text{U-GEDAN}(G, G') = \mathbf{P} \odot \left( \sum_{k=0}^K \mathbf{M}_k + \mathbf{B} + \mathbf{D} \right), \quad (9)$$

where U-GEDAN stands for *Unsupervised Graph Edit Distance Additive Network*. The U-GEDAN model is trained in an unsupervised manner to optimize its internal representations without access to ground truth distances. The corresponding loss is defined as

$$\omega^* = \arg \min_{\omega} \sum f_{\omega}(G, G'), \quad (10)$$

where  $\omega$  represents the parameters of the GNNs that produce the node representations  $h^{(k)}(v)$  and  $h^{(k)}(v')$  for the nodes  $v \in G$  and  $v' \in G'$ , respectively. U-GEDAN estimates the GED by leveraging the fact that it is zero if, and only if, two graphs are identical (see Eq. 4). This property provides an intrinsic learning signal, allowing the model to learn without external supervision. To further guide the learning process, we introduce injectivity constraints and apply regularization techniques, such as enforcing spherical embeddings when using cosine similarity (as shown in Eq. 2). The overall approach acts as a self-organizing system, where gradients derived from the GED objective help shape the internal representations, encouraging structural consistency across similar graphs.

In the U-GEDAN model, we do neither optimize the Gumbel-Sinkhorn network nor the deletion/insertion costs  $a^{\ominus}$ ,  $a^{\oplus}$ ,  $b^{\ominus}$ , and  $b^{\oplus}$ . Otherwise, one would risk that the network might exploit these components to trivially minimize the loss, thereby bypassing a meaningful learning of the representations.

### 2.3 S-GEDAN Model

For the second GED model, which is able to learn the costs, we define another series of  $(K + 1)$  matrices  $\mathbf{C}_k = (c_{ij})_{[n+m] \times [m+n]}$  where element  $c_{ij}$  encodes the result of a learnable cost function  $f_{\theta}^{(k)} : \tilde{V} \times \tilde{V}' \rightarrow \mathbb{R}_{>0}$  at level  $k$ . Formally,

$$\mathbf{C}_k = \left[ \begin{array}{ccc|cc} f^{(k)}(v_0, v'_0) & \dots & f^{(k)}(v_0, v'_m) & f^{(k)}(v_0, \epsilon) & \infty \\ \vdots & \ddots & \vdots & \ddots & \\ f^{(k)}(v_n, v'_0) & \dots & f^{(k)}(v_n, v'_m) & \infty & f^{(k)}(v_n, \epsilon) \\ \hline f^{(k)}(\epsilon, v'_0) & & \infty & & \\ & \ddots & & & 0 \\ \infty & & f^{(k)}(\epsilon, v'_m) & & \end{array} \right]. \quad (11)$$

where  $f_{\theta}^{(k)}$  takes the  $k$ -th representations  $h^{(k)}(v)$  and  $h^{(k)}(v')$  of two nodes  $v$  and  $v'$ , and produces a strictly positive value. Specifically, we use  $k$  MLPs with a softplus activation function ( $\beta = 5$ ) to model the cost values.

By making use of the soft permutation matrix  $\mathbf{P}$  as described in Eq. 8, we define the second – now supervised – approximation of the GED by

$$\text{S-GEDAN}(G, G') = \mathbf{P} \odot \left[ \lambda_1 \left( \sum_{k=0}^K \mathbf{M}_k + \mathbf{B} + \mathbf{D} \right) + \lambda_2 \left( \sum_{k=0}^K (\mathbf{M}_k \odot \mathbf{C}_k \cdot \beta_k) \right) \right], \quad (12)$$

where  $\beta_k$  are learnable scalars controlling the contribution of each level  $k$  and  $\lambda_1$  and  $\lambda_2$  are two scalars that modulate the impact of costs.

Table 1: Average and standard derivation of the error and correlation of GED approximations to exact GED obtained with six different configurations. The best results per dataset and metric is highlighted in boldface.

MODEL	AIDS [36]			MUTAG [36]			PTC MR [36]		
	RMSE	$\tau$	$\rho$	RMSE	$\tau$	$\rho$	RMSE	$\tau$	$\rho$
SimGNN (2019) [15]	8.72 ± 3.40	0.549 ± 0.03	0.760 ± 0.05	9.66 ± 2.96	0.582 ± 0.08	0.786 ± 0.10	8.57 ± 3.49	0.689 ± 0.07	<b>0.862 ± 0.06</b>
GREED (2022) [16]	<b>3.05 ± 0.08</b>	0.429 ± 0.08	0.633 ± 0.07	4.87 ± 0.48	<b>0.585 ± 0.04</b>	0.643 ± 0.06	<b>2.59 ± 0.43</b>	0.690 ± 0.02	0.859 ± 0.02
ERIC (2022) [17]	9.48 ± 3.01	0.484 ± 0.06	0.684 ± 0.09	9.68 ± 3.42	0.530 ± 0.07	0.748 ± 0.10	9.60 ± 3.31	0.665 ± 0.06	0.822 ± 0.06
GraphEdXxor (2024) [18]	8.06 ± 2.50	<b>0.560 ± 0.03</b>	<b>0.786 ± 0.05</b>	<b>4.61 ± 0.59</b>	0.570 ± 0.03	0.761 ± 0.07	4.40 ± 0.95	0.660 ± 0.04	0.828 ± 0.04
U-GEDAN	5.19 ± 1.39	0.436 ± 0.03	0.658 ± 0.03	10.18 ± 3.82	0.578 ± 0.04	0.813 ± 0.04	4.91 ± 1.34	0.664 ± 0.04	0.841 ± 0.03
S-GEDAN	4.58 ± 1.33	0.477 ± 0.03	0.696 ± 0.03	4.63 ± 0.99	0.579 ± 0.03	<b>0.818 ± 0.04</b>	4.44 ± 1.32	<b>0.693 ± 0.05</b>	0.856 ± 0.04

S-GEDAN enables the model to adaptively weigh the importance of each scale  $k$  and dynamically adjust the edit costs based on learned node representations. This stands in contrast to traditional approaches to GED approximation, which typically assign fixed scalar costs to edit operations, independent of the node or edge types. Moreover, previous methods [29] offer only indirect attempts to learn edit costs (e.g., via genetic algorithms), lacking both direct optimization and differentiability. In contrast, our method learns edit costs directly within a fully differentiable framework.

In order to approximate GED values, S-GEDAN is trained using explicit ground-truth distances, with the objective of minimizing the Smooth L1 [30] between the predicted and true distances. During training of S-GEDAN, we do not optimize the Gumbel-Sinkhorn network; instead, it is kept fixed to encourage the model to focus exclusively on learning the cost functions  $f_{\theta}^{(k)}$  and generating meaningful cost matrices  $\mathbf{C}_k$ . These matrices capture structural and semantic similarities between graphs, guided by their interaction with the learned dissimilarity matrices  $\mathbf{M}_k$ . The element-wise multiplication between  $\mathbf{C}_k$  and  $\mathbf{M}_k$  ensures that, despite  $f_{\theta}^{(k)}$  producing strictly positive values, the total cost vanishes in the case of a perfect matching.

## 2.4 Learning the Edit Costs of GED

The optimization of edit costs is carried out exclusively within the S-GEDAN framework, adopting a multi-task learning strategy [31], which involves the use of multiple loss functions. Multi-loss training in the context of metric learning has been extensively explored [32, 33], and is known to enhance generalization and improve the robustness of the learned representations. In our model two complementary loss functions are employed.

The first is a *Softmax-based Contrastive Loss* [34], which enables distance-based ranking without requiring an explicit margin. Given a query graph  $G_Q$  as well as one positive key  $G_P$  and  $M$  negative keys  $G_{N_1}, \dots, G_{N_M}$  (i.e., a graph  $G_P$  that is semantically similar to  $G_Q$ , and  $M$  graphs that are semantically dissimilar to  $G_Q$ ), the objective is to enforce that the GED between  $G_Q$  and  $G_P$  is lower than the GED between  $G_Q$  and each of the  $M$  negative keys  $G_{N_1}, \dots, G_{N_M}$ . Formally,

$$\text{GED}(G_Q, G_P) < \text{GED}(G_Q, G_{N_i}) \quad \forall i \in [1, \dots, M]. \quad (13)$$

This formulation encourages the model to learn edit costs that reflect semantic similarity by reducing the distance to the positive key and increasing it with respect to negative ones.

The second loss function is introduced to supervise the downstream task [35], which may involve either regression or classification. This loss is computed via a neural network module that processes the predicted GEDs between the query graph and a set of key graphs, and uses this information to predict the label of the query graph.

## 3 Experimental Evaluation

In this section we present the results obtained in three different experiments. The first evaluation aims at testing whether the novel model is able to approximate GED with sufficient accuracy in different cost scenarios. The second evaluation aims at empirically proving that the S-GEDAN with learned costs is more informative than U-GEDAN with fixed costs. Finally, in a third experiment, we show and discuss a use case of direct comparisons of molecular graphs using our model and the learned cost.

For the first experiment, we use three datasets from the TUDataset repository [36] that contain molecule graphs. The chosen datasets consist of intentionally small graphs, motivated by the need to

Table 2: Metrics obtained on the predicted embeddings: the table shows average values and their standard deviations. The best results are highlighted in bold.

	FreeSolv [40]		BBBP [41]		ZINC [42]	
	$R^2(\uparrow)$		ROC-AUC ( $\uparrow$ )		MAE ( $\downarrow$ )	
	Grid Search	Learned	Grid Search	Learned	Grid Search	Learned
KNN	0.270 $\pm$ 0.05	<b>0.542 <math>\pm</math> 0.04</b>	0.672 $\pm$ 0.04	<b>0.708 <math>\pm</math> 0.03</b>	1.451 $\pm$ 0.12	<b>0.945 <math>\pm</math> 0.09</b>
SVM	0.351 $\pm$ 0.04	<b>0.632 <math>\pm</math> 0.08</b>	0.685 $\pm$ 0.03	<b>0.692 <math>\pm</math> 0.02</b>	1.352 $\pm$ 0.09	<b>0.856 <math>\pm</math> 0.12</b>
RF	0.395 $\pm$ 0.06	<b>0.678 <math>\pm</math> 0.08</b>	0.666 $\pm$ 0.03	<b>0.696 <math>\pm</math> 0.03</b>	1.387 $\pm$ 0.07	<b>0.925 <math>\pm</math> 0.09</b>
MLP	0.320 $\pm$ 0.04	<b>0.701 <math>\pm</math> 0.09</b>	0.684 $\pm$ 0.05	<b>0.739 <math>\pm</math> 0.05</b>	1.315 $\pm$ 0.15	<b>0.921 <math>\pm</math> 0.13</b>

ensure the feasibility of the supervised training required by most models. For the second and third evaluation, we use three more benchmark datasets [37, 38], viz. FreeSolv, BBBP, and ZINC. The three datasets represent molecules describing hydration free energy, permeability of the blood-brain barrier, and restricted solubility (termed logP).

### 3.1 Approximation of Graph Edit Distance

In the first experiment we evaluate the quality of the novel GED approximations obtained by S-GEDAN and U-GEDAN and compare it with four state-of-the-art models that also approximate GED [15–18]. The quality of the different GED approximations is evaluated by the *Root Mean Square Error* (RMSE) to the exact GED as well as Kendall’s and Spearman’s correlation values  $\tau$  and  $\rho$ , respectively.

Table 1 shows the results obtained by the four reference models as well as the two versions of our model U-GEDAN and S-GEDAN. We report the mean and standard deviation of the results obtained with five different configurations<sup>1</sup>, highlighting the best result per dataset and metric in boldface.

Across all three datasets and metrics, results confirm the absence of a universally superior model [39]. S-GEDAN demonstrates competitive performance with the state of the art on nearly all metrics, with the highest  $\rho$  on MUTAG and the best  $\tau$  on PTC MR. Compared to S-GEDAN, U-GEDAN generally performs slightly worse, but its results remain close to the state-of-the-art results. This is an important result since all methods except U-GEDAN use ground truth distances for learning. The fact that the supervised methods perform better than U-GEDAN is therefore not surprising on the one hand, but again underlines their problem, namely the need to calculate a large number of ground truth distances on the training set, which is currently a bottleneck for all methods.

### 3.2 Optimization of Edit Costs

In this second experimental evaluation, we assess the effects of learning the edit costs using S-GEDAN. To date, no true baseline exists for direct comparison in this experimental setup. Supervised models for approximating the GED, including those used in our first experiment, are not directly applicable in our setting. This is due to two main reasons. First, computing the exact GED as ground truth is computationally prohibitive. Second—and more importantly—the edit costs that would enable effective modeling of the relationship between graph distances and target properties are not known a priori. Although theoretically applicable approaches, such genetic algorithms [29], encounter substantial computational challenges when optimizing continuous cost parameters for individual nodes or subgraphs, rendering them impractical for large-scale evaluation.

As a point of reference, we perform a constrained grid search using U-GEDAN, leveraging its ability to approximate GED without requiring ground truth. Specifically, we evaluate 16 cost configurations by setting insertion and deletion costs for nodes and edges to either 1 or 2, and report results for the best-performing setting.

We use the predicted GED of both U-GEDAN and S-GEDAN to embed the graphs in a vector space using dissimilarity-based embeddings [43]. The prototype selection (actually required for graph embedding) is performed uniformly for both models to ensure a fair comparison. Moreover, to

<sup>1</sup>These five different configurations represent five different combinations of fixed costs for deletions and insertions for both nodes and edges.

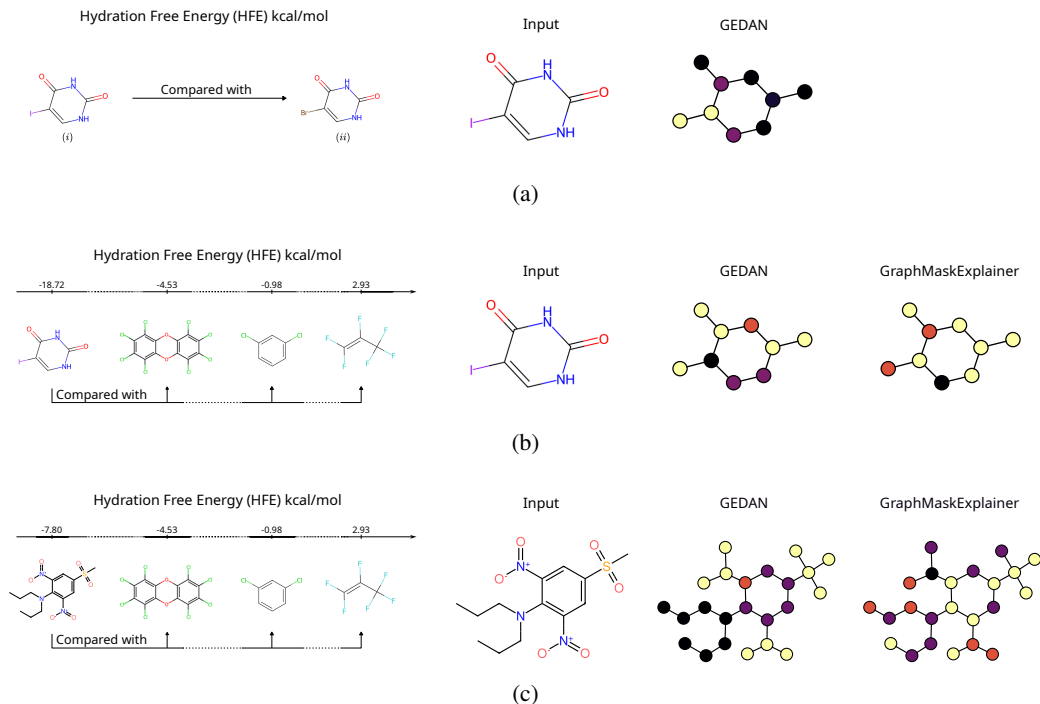


Figure 2: Cost analysis of our model compared to the model analyzed with GraphMaskExplainer [46] on the FreeSolv dataset. On the left (A) is a comparison with the entire dataset, on the right (B) is an example of direct comparison of our model on similar molecules.

ensure the robustness of our results and to avoid possible bias due to an unrepresentative selection of prototypes, we repeat the process three times (for each fold during cross-validation).

Due to the large number of graphs, we only select 16 prototypes from the training set for each dataset. This means that we ultimately obtain 16-dimensional embeddings for both the training set and the test set, on which we solve the underlying regression or classification problem of the three datasets using standard models – in particular we employ k-Nearest Neighbors (KNN), Support Vector Machines (SVM), Random Forest (RF) and Multi-Layer Perceptron (MLP). and evaluate their performance by means of  $R^2$ , ROC-AUC and MAE (note that we do not use the three metrics equally on all three datasets but use only one metric per dataset – this in line with common comparisons on the respective datasets [44]).

The results in Table 2 show that the learned cost leads to a more expressive GED compared to the grid search-defined cost. That is, the learned cost better captures the relationships between the graphs in relation to the graph properties and improves the model performance. In contrast, grid search optimization is not only computationally expensive, but also impractical because it is not possible to adequately model the continuous costs that the network learns.

Although the overall results are quite distant from the state of the art [45], it is important to note that the 16 prototypes used for embedding constitute only about 3% of the FreeSolv training set and less than 1% of the other data sets. The purpose of this analysis is to show that the effects of cost optimization are still clearly visible even with suboptimal graph embeddings.

### 3.3 Analysis of Edit Costs

One of the key advantages of our method is its ability to perform direct comparisons between graphs by analyzing the cost of transforming one graph into another. In the following analysis, we assume that higher transformation costs indicate higher relevance. Accordingly, we visualize the nodes using a color gradient where dark colors represent low-cost (i.e., low-relevance) transformations, while light colors represent high-cost (i.e., high-relevance) transformations.

There are several interpretation methods and inherently explainable architectures available. However, we focus on analyzing a GNN that achieves state-of-the-art performance [45] using GraphMaskExplainer [46]. This choice ensures consistent evaluation within a fixed model architecture, enabling us to focus on cost-based, globally coherent explanations. Alternative methods, such as GNNExplainer [47] and SubgraphX [48], use different interpretability paradigms (e.g., perturbation or subgraph identification), providing different types of insights. Additionally, other neural architectures, like GNAN [28], GAT [49], or GKAN [50], would require altering the underlying model, complicating direct comparisons.

The following three analyses are conducted on the FreeSolv dataset, with the goal of estimating hydration free energy (HFE). This analysis highlights the molecular substructures that contribute most significantly to the target property, HFE.

In Figure 2 (a), we show the results by comparing two specific molecules (marked (*i*) and (*ii*) in the figure), using S-GEDAN with respect to the HFE target. The two molecules are structurally similar; in particular, the substitution of an iodine atom (I) with a bromine atom (Br) leads to a slight change in HFE – only 0.55 kcal/mol — according to the target values. Hence, we expect the substitution of I for Br to be identified as significant, and the cost analysis of S-GEDAN confirms this by localizing the change responsible for the observed energy difference of 0.55 kcal/mol. This comparison is only possible with our approach but not with GraphMaskExplainer.

In Figure 2 (b), we visualize the transformation costs between the molecule (*i*) with respect to all graphs from the dataset. Both models, S-GEDAN and GraphMaskExplainer, correctly identify the two carbonyls as important for the target property. However, in contrast to GraphMaskExplainer, our model emphasizes the chemically relevant symmetry of the functional group formed by the two carbonyls. This symmetry arises because the edit costs depend on the correspondences of the nodes in the additive layers, which promotes consistency of predictions when the structures are similar.

In Figure 2 (c), we investigate a molecule containing functional groups known to enhance water solubility. Specifically, the sulfonyl and nitro groups ( $-\text{SO}_2-$  and  $-\text{NO}_2$ ), which are known to potentially influence solubility [51, 52], are correctly identified by our model. The model recognizes the groups as relevant, suggesting a differential contribution between these regions. In contrast, the comparison model only detects partial fragments of the key components, making its results difficult to interpret.

## 4 Conclusion

The computation of graph similarity is a computationally challenging problem, formally classified as NP-hard. Recent developments, particularly in the domain of GNNs, have enabled more scalable approximation techniques, advancing the feasibility of applying graph similarity in real-world scenarios.

In this paper, we introduce a novel graph-based architecture that optimizes transformation costs in graph matching with respect to a target variable. This addresses a known limitation of related techniques that operate with unit costs. Furthermore, the proposed method can learn matching relationships in an unsupervised manner, removing the need for prior ground-truth distances (a known bottleneck of current methods). In an experimental evaluation, we show that our method achieves competitive performance with the current state of the art. Moreover, our approach enables meaningful identification of highly relevant nodes and/or subgraphs in specific graphs. Highlighting these regions offers great potential to help experts to extract additional information from the underlying graphs. In future work, we aim to increase the maximum size of the processable graphs by placing more emphasis on scalability.

**Limitations** Our method has at least three major limitations. First, GEDAN incurs higher computational complexity compared to state-of-the-art approaches. This is due to two reasons. First, the overhead introduced by managing pairwise cost and matching matrices, and second the introduction of a padding to handle different graph sizes. Despite optimizations such as broadcasting, the computation and storage of these matrices result in an increased runtime and memory consumption. The second limitation is the number of nodes that can be processed efficiently by our model due to the constraints of the matrix operations resulting from the use of the Gumbel-Sinkhorn network. Our current study presents results on graphs with up to 64 nodes. However, the design of the Gumbel-

Sinkhorn network theoretically allows its application to graphs with thousands of nodes, although this may result in increased computational and memory complexity. The third limitation is the use of a single edge type. Actually, this might limit the model's ability to capture the full complexity of molecular structures, which often rely on multiple bond types to convey relational information.

## Acknowledgments and Disclosure of Funding

## References

- [1] Hongsong Chen. Networks, crowds, and markets: Reasoning about a highly connected world [book review]. *IEEE Technol. Soc. Mag.*, 32(3):10, 2013. doi: 10.1109/MTS.2013.2276667. URL <https://doi.org/10.1109/MTS.2013.2276667>.
- [2] Alexander Mathis, Pranav Mamidanna, Kevin M Cury, Taiga Abe, Venkatesh N Murthy, Mackenzie Weygandt Mathis, and Matthias Bethge. Deeplabcut: markerless pose estimation of user-defined body parts with deep learning. *Nature neuroscience*, 21(9):1281–1289, 2018.
- [3] Mordechai (Muki) Haklay and Patrick Weber. Openstreetmap: User-generated street maps. *IEEE Pervasive Comput.*, 7(4):12–18, 2008. doi: 10.1109/MPRV.2008.80. URL <https://doi.org/10.1109/MPRV.2008.80>.
- [4] Benjamin Fankhauser, Vidushi Bigler, and Kaspar Riesen. Spatio-temporal graph neural networks for water temperature modeling. In Andrea Torsello, Luca Rossi, Luca Cosmo, and Giorgia Minello, editors, *Structural, Syntactic, and Statistical Pattern Recognition - Joint IAPR International Workshops, S+SSPR 2024, Venice, Italy, September 9-10, 2024, Revised Selected Papers*, volume 15444 of *Lecture Notes in Computer Science*, pages 31–40. Springer, 2024. doi: 10.1007/978-3-031-80507-3\_4. URL [https://doi.org/10.1007/978-3-031-80507-3\\_4](https://doi.org/10.1007/978-3-031-80507-3_4).
- [5] Frances C Bernstein, Thomas F Koetzle, Grahame JB Williams, Edgar F Meyer Jr, Michael D Brice, John R Rodgers, Olga Kennard, Takehiko Shimanouchi, and Mitsuo Tasumi. The protein data bank: a computer-based archival file for macromolecular structures. *Journal of molecular biology*, 112(3):535–542, 1977.
- [6] A. Patrícia Bento, Anne Hersey, Eloy Felix, Gregory A. Landrum, Anna Gaulton, Francis Atkinson, Louisa J. Bellis, Marleen De Veij, and Andrew R. Leach. An open source chemical structure curation pipeline using rdkit. *J. Cheminformatics*, 12(1):51, 2020. doi: 10.1186/S13321-020-00456-1. URL <https://doi.org/10.1186/s13321-020-00456-1>.
- [7] Donatello Conte, Pasquale Foggia, Carlo Sansone, and Mario Vento. Thirty years of graph matching in pattern recognition. *Int. J. Pattern Recognit. Artif. Intell.*, 18(3):265–298, 2004. doi: 10.1142/S0218001404003228. URL <https://doi.org/10.1142/S0218001404003228>.
- [8] Xinbo Gao, Bing Xiao, Dacheng Tao, and Xuelong Li. A survey of graph edit distance. *Pattern Anal. Appl.*, 13(1):113–129, 2010. doi: 10.1007/S10044-008-0141-Y. URL <https://doi.org/10.1007/s10044-008-0141-y>.
- [9] Alfred V. Aho, John E. Hopcroft, and Jeffrey D. Ullman. *The Design and Analysis of Computer Algorithms*. Addison-Wesley, 1974. ISBN 0-201-00029-6.
- [10] Derek Justice and Alfred O. Hero III. A binary linear programming formulation of the graph edit distance. *IEEE Trans. Pattern Anal. Mach. Intell.*, 28(8):1200–1214, 2006. doi: 10.1109/TPAMI.2006.152. URL <https://doi.org/10.1109/TPAMI.2006.152>.
- [11] Michel Neuhaus, Kaspar Riesen, and Horst Bunke. Fast suboptimal algorithms for the computation of graph edit distance. In Dit-Yan Yeung, James T. Kwok, Ana L. N. Fred, Fabio Roli, and Dick de Ridder, editors, *Structural, Syntactic, and Statistical Pattern Recognition, Joint IAPR International Workshops, SSPR 2006 and SPR 2006, Hong Kong, China, August 17-19, 2006, Proceedings*, volume 4109 of *Lecture Notes in Computer Science*, pages 163–172. Springer, 2006. doi: 10.1007/11815921\_17. URL [https://doi.org/10.1007/11815921\\_17](https://doi.org/10.1007/11815921_17).

- [12] Kaspar Riesen and Horst Bunke. Approximate graph edit distance computation by means of bipartite graph matching. *Image Vis. Comput.*, 27(7):950–959, 2009. doi: 10.1016/J.IMAVIS.2008.04.004. URL <https://doi.org/10.1016/j.imavis.2008.04.004>.
- [13] Sébastien Bougleux, Luc Brun, Vincenzo Carletti, Pasquale Foggia, Benoit Gaüzère, and Mario Vento. Graph edit distance as a quadratic assignment problem. *Pattern Recognit. Lett.*, 87: 38–46, 2017. doi: 10.1016/J.PATREC.2016.10.001. URL <https://doi.org/10.1016/j.patrec.2016.10.001>.
- [14] Nicolas Boria, David B. Blumenthal, Sébastien Bougleux, and Luc Brun. Improved local search for graph edit distance. *Pattern Recognit. Lett.*, 129:19–25, 2020. doi: 10.1016/J.PATREC.2019.10.028. URL <https://doi.org/10.1016/j.patrec.2019.10.028>.
- [15] Yunsheng Bai, Hao Ding, Song Bian, Ting Chen, Yizhou Sun, and Wei Wang. Simgnn: A neural network approach to fast graph similarity computation. In J. Shane Culpepper, Alistair Moffat, Paul N. Bennett, and Kristina Lerman, editors, *Proceedings of the Twelfth ACM International Conference on Web Search and Data Mining, WSDM 2019, Melbourne, VIC, Australia, February 11-15, 2019*, pages 384–392. ACM, 2019. doi: 10.1145/3289600.3290967. URL <https://doi.org/10.1145/3289600.3290967>.
- [16] Rishabh Ranjan, Siddharth Grover, Sourav Medya, Venkatesan T. Chakaravarthy, Yogish Sabharwal, and Sayan Ranu. GREED: A neural framework for learning graph distance functions. In Sanmi Koyejo, S. Mohamed, A. Agarwal, Danielle Belgrave, K. Cho, and A. Oh, editors, *Advances in Neural Information Processing Systems 35: Annual Conference on Neural Information Processing Systems 2022, NeurIPS 2022, New Orleans, LA, USA, November 28 - December 9, 2022*, 2022. URL [http://papers.nips.cc/paper\\_files/paper/2022/hash/8d492b8a6201d83d1015af9e264f0bf2-Abstract-Conference.html](http://papers.nips.cc/paper_files/paper/2022/hash/8d492b8a6201d83d1015af9e264f0bf2-Abstract-Conference.html).
- [17] Wei Zhuo and Guang Tan. Efficient graph similarity computation with alignment regularization. 2022. URL [http://papers.nips.cc/paper\\_files/paper/2022/hash/c2ce2f2701c10a2b2f2ea0bfa43cfaa3-Abstract-Conference.html](http://papers.nips.cc/paper_files/paper/2022/hash/c2ce2f2701c10a2b2f2ea0bfa43cfaa3-Abstract-Conference.html).
- [18] Eeshaan Jain, Indradyumna Roy, Saswat Meher, Soumen Chakrabarti, and Abir De. Graph edit distance with general costs using neural set divergence. In Amir Globersons, Lester Mackey, Danielle Belgrave, Angela Fan, Ulrich Paquet, Jakub M. Tomczak, and Cheng Zhang, editors, *Advances in Neural Information Processing Systems 38: Annual Conference on Neural Information Processing Systems 2024, NeurIPS 2024, Vancouver, BC, Canada, December 10 - 15, 2024*, 2024. URL [http://papers.nips.cc/paper\\_files/paper/2024/hash/860e5b214c842eaedaa6b4026ee91aac-Abstract-Conference.html](http://papers.nips.cc/paper_files/paper/2024/hash/860e5b214c842eaedaa6b4026ee91aac-Abstract-Conference.html).
- [19] Peilun Yang, Hanchen Wang, Jianye Yang, Zhengping Qian, Ying Zhang, and Xuemin Lin. Deep learning approaches for similarity computation: A survey. *IEEE Trans. Knowl. Data Eng.*, 36(12):7893–7912, 2024. doi: 10.1109/TKDE.2024.3422484. URL <https://doi.org/10.1109/TKDE.2024.3422484>.
- [20] Anne AY Guilbert, Zachary S Parr, Theo Kreouzis, Duncan J Woods, Reiner Sebastian Sprick, Isaac Abrahams, Christian B Nielsen, and Mohamed Zbiri. Effect of substituting non-polar chains with polar chains on the structural dynamics of small organic molecule and polymer semiconductors. *Physical Chemistry Chemical Physics*, 23(12):7462–7471, 2021.
- [21] Joshua Edzards, Holger-Dietrich Saßnick, Julia Santana Andreo, and Caterina Cocchi. Tuning structural and electronic properties of metal-organic framework 5 by metal substitution and linker functionalization. *The Journal of Chemical Physics*, 160(18), 2024.
- [22] Zonghan Wu, Shirui Pan, Fengwen Chen, Guodong Long, Chengqi Zhang, and Philip S. Yu. A comprehensive survey on graph neural networks. *IEEE Trans. Neural Networks Learn. Syst.*, 32(1):4–24, 2021. doi: 10.1109/TNNLS.2020.2978386. URL <https://doi.org/10.1109/TNNLS.2020.2978386>.
- [23] Daniel F. McCaffrey. Generalized additive models (T. j. hastie and r. j. tibshirani). volume 34, pages 675–678. 1992. doi: 10.1137/1034142. URL <https://doi.org/10.1137/1034142>.

- [24] Gonzalo E. Mena, David Belanger, Scott W. Linderman, and Jasper Snoek. Learning latent permutations with gumbel-sinkhorn networks. 2018. URL <https://openreview.net/forum?id=Byt3oJ-0W>.
- [25] Keyulu Xu, Weihua Hu, Jure Leskovec, and Stefanie Jegelka. How powerful are graph neural networks? In *7th International Conference on Learning Representations, ICLR 2019, New Orleans, LA, USA, May 6-9, 2019*. OpenReview.net, 2019. URL <https://openreview.net/forum?id=ryGs6iA5Km>.
- [26] Nino Shervashidze, Pascal Schweitzer, Erik Jan van Leeuwen, Kurt Mehlhorn, and Karsten M. Borgwardt. Weisfeiler-lehman graph kernels. *J. Mach. Learn. Res.*, 12:2539–2561, 2011. doi: 10.5555/1953048.2078187. URL <https://dl.acm.org/doi/10.5555/1953048.2078187>.
- [27] Michael Scholkemper, Xinyi Wu, Ali Jadbabaie, and Michael T. Schaub. Residual connections and normalization can provably prevent oversmoothing in gnns. *CoRR*, abs/2406.02997, 2024. doi: 10.48550/ARXIV.2406.02997. URL <https://doi.org/10.48550/arXiv.2406.02997>.
- [28] Maya Bechler-Speicher, Amir Globerson, and Ran Gilad-Bachrach. The intelligible and effective graph neural additive network. 2024. URL [http://papers.nips.cc/paper\\_files/paper/2024/hash/a4c3a66ed818455b8bbe591b6a5d0f56-Abstract-Conference.html](http://papers.nips.cc/paper_files/paper/2024/hash/a4c3a66ed818455b8bbe591b6a5d0f56-Abstract-Conference.html).
- [29] Carlos Garcia-Hernandez, Alberto Fernández, and Francesc Serratos. Learning the edit costs of graph edit distance applied to ligand-based virtual screening. *Current topics in medicinal chemistry*, 20(18):1582–1592, 2020.
- [30] Ross B. Girshick. Fast R-CNN. In *2015 IEEE International Conference on Computer Vision, ICCV 2015, Santiago, Chile, December 7-13, 2015*, pages 1440–1448. IEEE Computer Society, 2015. doi: 10.1109/ICCV.2015.169. URL <https://doi.org/10.1109/ICCV.2015.169>.
- [31] Hyun Oh Song, Yu Xiang, Stefanie Jegelka, and Silvio Savarese. Deep metric learning via lifted structured feature embedding. In *2016 IEEE Conference on Computer Vision and Pattern Recognition, CVPR 2016, Las Vegas, NV, USA, June 27-30, 2016*, pages 4004–4012. IEEE Computer Society, 2016. doi: 10.1109/CVPR.2016.434. URL <https://doi.org/10.1109/CVPR.2016.434>.
- [32] Xinshao Wang, Yang Hua, Elyor Kodirov, Guosheng Hu, Romain Garnier, and Neil Martin Robertson. Ranked list loss for deep metric learning. In *IEEE Conference on Computer Vision and Pattern Recognition, CVPR 2019, Long Beach, CA, USA, June 16-20, 2019*, pages 5207–5216. Computer Vision Foundation / IEEE, 2019. doi: 10.1109/CVPR.2019.00535. URL [http://openaccess.thecvf.com/content\\_CVPR\\_2019/html/Wang\\_Ranked\\_List\\_Loss\\_for\\_Deep\\_Metric\\_Learning\\_CVPR\\_2019\\_paper.html](http://openaccess.thecvf.com/content_CVPR_2019/html/Wang_Ranked_List_Loss_for_Deep_Metric_Learning_CVPR_2019_paper.html).
- [33] Florian Schroff, Dmitry Kalenichenko, and James Philbin. Facenet: A unified embedding for face recognition and clustering. In *IEEE Conference on Computer Vision and Pattern Recognition, CVPR 2015, Boston, MA, USA, June 7-12, 2015*, pages 815–823. IEEE Computer Society, 2015. doi: 10.1109/CVPR.2015.7298682. URL <https://doi.org/10.1109/CVPR.2015.7298682>.
- [34] Xun Wang, Xintong Han, Weilin Huang, Dengke Dong, and Matthew R. Scott. Multi-similarity loss with general pair weighting for deep metric learning. In *IEEE Conference on Computer Vision and Pattern Recognition, CVPR 2019, Long Beach, CA, USA, June 16-20, 2019*, pages 5022–5030. Computer Vision Foundation / IEEE, 2019. doi: 10.1109/CVPR.2019.00516. URL [http://openaccess.thecvf.com/content\\_CVPR\\_2019/html/Wang\\_Multi-Similarity\\_Loss\\_With\\_General\\_Pair\\_Weighting\\_for\\_Deep\\_Metric\\_Learning\\_CVPR\\_2019\\_paper.html](http://openaccess.thecvf.com/content_CVPR_2019/html/Wang_Multi-Similarity_Loss_With_General_Pair_Weighting_for_Deep_Metric_Learning_CVPR_2019_paper.html).
- [35] Vlad Sobal, Mark Ibrahim, Randall Balestriero, Vivien Cabannes, Diane Bouchacourt, Pietro Astolfi, Kyunghyun Cho, and Yann LeCun.  $\mathbb{X}$ -sample contrastive loss: Improving contrastive learning with sample similarity graphs. *CoRR*, abs/2407.18134, 2024. doi: 10.48550/ARXIV.2407.18134. URL <https://doi.org/10.48550/arXiv.2407.18134>.

- [36] Christopher Morris, Nils M. Kriege, Franka Bause, Kristian Kersting, Petra Mutzel, and Marion Neumann. Tudataset: A collection of benchmark datasets for learning with graphs. *CoRR*, abs/2007.08663, 2020. URL <https://arxiv.org/abs/2007.08663>.
- [37] Zhenqin Wu, Bharath Ramsundar, Evan N. Feinberg, Joseph Gomes, Caleb Geniesse, Aneesh S. Pappu, Karl Leswing, and Vijay S. Pande. Moleculenet: A benchmark for molecular machine learning. *CoRR*, abs/1703.00564, 2017. URL <http://arxiv.org/abs/1703.00564>.
- [38] Vijay Prakash Dwivedi, Chaitanya K. Joshi, Anh Tuan Luu, Thomas Laurent, Yoshua Bengio, and Xavier Bresson. Benchmarking graph neural networks. *J. Mach. Learn. Res.*, 24:43:1–43:48, 2023. URL <https://jmlr.org/papers/v24/22-0567.html>.
- [39] David H. Wolpert and William G. Macready. No free lunch theorems for optimization. *IEEE Trans. Evol. Comput.*, 1(1):67–82, 1997. doi: 10.1109/4235.585893. URL <https://doi.org/10.1109/4235.585893>.
- [40] David L. Mobley and J. Peter Guthrie. Freesolv: a database of experimental and calculated hydration free energies, with input files. *J. Comput. Aided Mol. Des.*, 28(7):711–720, 2014. doi: 10.1007/S10822-014-9747-X. URL <https://doi.org/10.1007/s10822-014-9747-x>.
- [41] Ines Filipa Martins, Ana L. Teixeira, Luis Pinheiro, and André O. Falcão. A bayesian approach to *in Silico* blood-brain barrier penetration modeling. *J. Chem. Inf. Model.*, 52(6):1686–1697, 2012. doi: 10.1021/CI300124C. URL <https://doi.org/10.1021/ci300124c>.
- [42] Rafael Gómez-Bombarelli, David Duvenaud, José Miguel Hernández-Lobato, Jorge Aguilera-Iparraguirre, Timothy D. Hirzel, Ryan P. Adams, and Alán Aspuru-Guzik. Automatic chemical design using a data-driven continuous representation of molecules. *CoRR*, abs/1610.02415, 2016. URL <http://arxiv.org/abs/1610.02415>.
- [43] Elzbieta Pekalska and Robert P. W. Duin. *The Dissimilarity Representation for Pattern Recognition - Foundations and Applications*, volume 64 of *Series in Machine Perception and Artificial Intelligence*. WorldScientific, 2005. ISBN 978-981-256-530-3. doi: 10.1142/5965. URL <https://doi.org/10.1142/5965>.
- [44] Kun Xu, Lingfei Wu, Zhiguo Wang, Yansong Feng, and Vadim Sheinin. Graph2seq: Graph to sequence learning with attention-based neural networks. *CoRR*, abs/1804.00823, 2018. URL <http://arxiv.org/abs/1804.00823>.
- [45] David Buterez, Jon Paul Janet, Dino Oglic, and Pietro Lio. Masked attention is all you need for graphs. *CoRR*, abs/2402.10793, 2024. doi: 10.48550/ARXIV.2402.10793. URL <https://doi.org/10.48550/arXiv.2402.10793>.
- [46] Michael Sejr Schlichtkrull, Nicola De Cao, and Ivan Titov. Interpreting graph neural networks for NLP with differentiable edge masking. 2021. URL <https://openreview.net/forum?id=WznmQa42ZAx>.
- [47] Zhitao Ying, Dylan Bourgeois, Jiaxuan You, Marinka Zitnik, and Jure Leskovec. Gnnexplainer: Generating explanations for graph neural networks. In Hanna M. Wallach, Hugo Larochelle, Alina Beygelzimer, Florence d’Alché-Buc, Emily B. Fox, and Roman Garnett, editors, *Advances in Neural Information Processing Systems 32: Annual Conference on Neural Information Processing Systems 2019, NeurIPS 2019, December 8-14, 2019, Vancouver, BC, Canada*, pages 9240–9251, 2019. URL <https://proceedings.neurips.cc/paper/2019/hash/d80b7040b773199015de6d3b4293c8ff-Abstract.html>.
- [48] Hao Yuan, Haiyang Yu, Jie Wang, Kang Li, and Shuiwang Ji. On explainability of graph neural networks via subgraph explorations. In Marina Meila and Tong Zhang, editors, *Proceedings of the 38th International Conference on Machine Learning, ICML 2021, 18-24 July 2021, Virtual Event*, volume 139 of *Proceedings of Machine Learning Research*, pages 12241–12252. PMLR, 2021. URL <http://proceedings.mlr.press/v139/yuan21c.html>.
- [49] Shaked Brody, Uri Alon, and Eran Yahav. How attentive are graph attention networks? 2022. URL <https://openreview.net/forum?id=F72ximsx7C1>.

- [50] Mehrdad Kiamari, Mohammad Kiamari, and Bhaskar Krishnamachari. GKAN: graph kolmogorov-arnold networks. *CoRR*, abs/2406.06470, 2024. doi: 10.48550/ARXIV.2406.06470. URL <https://doi.org/10.48550/arXiv.2406.06470>.
- [51] R N Goldberg and V B Parker. Thermodynamics of solution of  $\text{so}_2(\text{g})$  in water and of aqueous sulfur dioxide solutions. *Journal of research of the National Bureau of Standards (1977)*, 90(5): 341–358, 1985. ISSN 0160-1741. doi: 10.6028/jres.090.024. URL <https://pubmed.ncbi.nlm.nih.gov/34566163/>.
- [52] Robert Thornton Morrison and Robert Neilson Boyd. *Organic Chemistry*. Prentice Hall, Englewood Cliffs, NJ, 6 edition, 1992.
- [53] George H Dunteman. *Principal components analysis*, volume 69. Sage, 1989.
- [54] Rushi Shah, Mingyuan Yan, Michael Curtis Mozer, and Dianbo Liu. Improving discrete optimisation via decoupled straight-through gumbel-softmax. *CoRR*, abs/2410.13331, 2024. doi: 10.48550/ARXIV.2410.13331. URL <https://doi.org/10.48550/arXiv.2410.13331>.
- [55] MW Neamah and BA Qasim. A new left truncated gumbel distribution: Properties and estimation. In *Journal of physics: conference Series*, volume 1897, page 012015. IOP Publishing, 2021.
- [56] Iris A. M. Huijben, Wouter Kool, Max B. Paulus, and Ruud J. G. van Sloun. A review of the gumbel-max trick and its extensions for discrete stochasticity in machine learning. *IEEE Trans. Pattern Anal. Mach. Intell.*, 45(2):1353–1371, 2023. doi: 10.1109/TPAMI.2022.3157042. URL <https://doi.org/10.1109/TPAMI.2022.3157042>.
- [57] Richard Sinkhorn. A relationship between arbitrary positive matrices and doubly stochastic matrices. *The annals of mathematical statistics*, 35(2):876–879, 1964.
- [58] Yann LeCun, Léon Bottou, Yoshua Bengio, and Patrick Haffner. Gradient-based learning applied to document recognition. *Proc. IEEE*, 86(11):2278–2324, 1998. doi: 10.1109/5.726791. URL <https://doi.org/10.1109/5.726791>.

## A Details on the formulation of GEDAN

In this section we detail the two GEDAN models, supervised S-GEDAN and unsupervised U-GEDAN. Let  $G = (V, E, \mu)$  and  $G' = (V', E', \mu')$  be two graphs, padded with  $n = |V'|$  and  $m = |V|$  dummy nodes termed  $\epsilon$ , which are all assigned a special label  $\mu(\epsilon)$ . Let  $\tilde{V} = V \cup \{\epsilon\}_{|V'|}$  and  $\tilde{V}' = V' \cup \{\epsilon\}_{|V|}$  be the sets of nodes of the padded graphs. Formally, the our model GEDAN uses four matrices. The first matrix,  $\mathbf{B}$ , encodes the insertion  $a^\oplus$  and deletion  $a^\ominus$  costs for nodes. Formally, it is defined as:

$$\mathbf{B} = \left[ \begin{array}{cc|cc} & & a^\ominus & \infty \\ & 0 & & \ddots \\ a^\oplus & \infty & \infty & a^\ominus \\ & \ddots & & \\ \infty & a^\oplus & & 0 \end{array} \right]. \quad (14)$$

The second matrix,  $\mathbf{D}$ , captures the insertion  $b^\oplus$  and deletion  $b^\ominus$  costs for edges, computed as:

$$d_{ij} = \text{ReLU}(\deg(v_i) - \deg(v'_j)) \cdot b^\ominus + \text{ReLU}(\deg(v'_j) - \deg(v_i)) \cdot b^\oplus. \quad (15)$$

The corresponding matrix  $\mathbf{D}$  is formally defined as:

$$\mathbf{D} = \left[ \begin{array}{ccc|cc} \text{dg}(v_0, v'_0) & \dots & \text{dg}(v_0, v'_m) & \text{dg}(v_0, \epsilon) & \infty \\ \vdots & \ddots & \vdots & & \ddots \\ \text{dg}(v_n, v'_0) & \dots & \text{dg}(v_n, v'_m) & \infty & \text{dg}(v_n, \epsilon) \\ \text{dg}(\epsilon, v'_0) & & \infty & & \\ & \ddots & & & \\ \infty & & \text{dg}(\epsilon, v'_m) & & 0 \end{array} \right]. \quad (16)$$

As introduced in the main text,  $\mathbf{M}_k$  denotes the matrix of pairwise node dissimilarities based on their  $k$ -hop representations, while  $\mathbf{C}_k$  contains learnable transformation costs between node embeddings at level  $k$ . We could extend this formulation into a temperature-scaled version by introducing a scalar  $\mathcal{T}$ , which is used to normalize the combined dissimilarity matrix  $\sum_{k=0}^K \mathbf{M}_k$ , and a weight normalization factor  $\beta_K = \sum_{k=0}^K \beta_k$  applied to the cost aggregation  $\sum_{k=0}^K \mathbf{C}_k$ .

As defined in the main body, we use a pre-trained Gumbel-Sinkhorn network [24] to compute a soft permutation matrix  $\mathbf{P}$ . Incorporating temperature, this becomes:

$$\mathbf{P} = \text{Gumbel-Sinkhorn} \left[ \left( \sum_{k=0}^K \mathbf{M}_k \right) \cdot \frac{1}{\mathcal{T}} + \mathbf{B} + \mathbf{D} \right], \quad (17)$$

The unsupervised model, U-GEDAN, is defined as:

$$\text{U-GEDAN}(G, G') = \mathbf{P} \odot \left[ \left( \sum_{k=0}^K \mathbf{M}_k \right) \cdot \frac{1}{\mathcal{T}} + \mathbf{B} + \mathbf{D} \right] + \lambda_{\mathcal{T}} \cdot \log(\mathcal{T}). \quad (18)$$

The supervised model, S-GEDAN, is defined as:

$$\text{S-GEDAN}(G, G') = \mathbf{P} \odot \left[ \lambda_1 \left( \sum_{k=0}^K \mathbf{M}_k \right) \cdot \frac{1}{\mathcal{T}} + \mathbf{B} + \mathbf{D} \right] + \lambda_2 \left( \sum_{k=0}^K (\mathbf{M}_k \odot \mathbf{C}_k \cdot \beta_k) \cdot \frac{1}{\beta_K} \right) + \lambda_{\mathcal{T}} \cdot \log(\mathcal{T}). \quad (19)$$

where  $\lambda_{\mathcal{T}}$  modulates the effect of the logarithm of the temperature  $\mathcal{T}$ .

### A.1 Layer Influence and Inference Dynamics

In this section, we demonstrate how increasing the number of layers and optimizing their structure can lead to improved GED prediction. As suggested by Eq. 4, the hyperparameter  $K$  plays a crucial role by controlling the receptive field size over the graph. A higher value of  $K$  allows the model to capture more structural information, which should, in principle, lead to better graph-aware predictions.

To isolate the effect of architectural depth, we conduct a first experiment using U-GEDAN in a purely inference setting, without any prior training. As shown in Table 3, increasing  $K$  leads to both a higher parameter and consistent improvements in rank-based metrics  $\tau$  and  $\rho$ . This suggests enhanced alignment with the underlying graph structure. However, this increase in structural coherence does not directly translate to better RMSE performance. We hypothesize that this is due to the nature of the injective  $A^k$  layers, which are implemented as non-linear GIN layers. While such  $K$  layers improve relational consistency, they do not necessarily minimize prediction error in an untrained setting.

Table 3: U-GEDAN inference of the GED approximation with  $K$ -layers on Configuration 1.

LAYERS		AIDS [36]			MUTAG [36]			PTC MR [36]		
K	Avg. Param.	RMSE	$\tau$	$\rho$	RMSE	$\tau$	$\rho$	RMSE	$\tau$	$\rho$
1	6K	<b>6.71 ± 0.07</b>	0.384 ± 0.07	0.600 ± 0.07	11.52 ± 0.74	0.602 ± 0.09	0.844 ± 0.05	<b>4.92 ± 0.52</b>	0.585 ± 0.08	0.785 ± 0.06
2	8K	6.79 ± 0.13	0.393 ± 0.07	0.609 ± 0.07	11.77 ± 0.80	0.605 ± 0.09	0.848 ± 0.04	4.96 ± 0.52	0.598 ± 0.08	0.795 ± 0.06
4	12K	6.80 ± 0.11	0.404 ± 0.07	0.609 ± 0.07	11.40 ± 0.93	0.612 ± 0.09	0.855 ± 0.04	5.26 ± 0.57	0.605 ± 0.08	0.801 ± 0.06
8	19K	7.20 ± 0.23	0.412 ± 0.07	0.630 ± 0.07	10.60 ± 0.89	0.618 ± 0.08	0.862 ± 0.04	5.70 ± 0.56	0.614 ± 0.07	0.809 ± 0.06
16	35K	7.48 ± 0.14	0.422 ± 0.07	0.638 ± 0.07	10.15 ± 0.93	0.618 ± 0.08	0.868 ± 0.03	6.17 ± 0.60	0.621 ± 0.08	0.814 ± 0.06
32	66K	7.91 ± 0.21	<b>0.430 ± 0.07</b>	<b>0.647 ± 0.07</b>	<b>9.29 ± 1.12</b>	<b>0.615 ± 0.08</b>	<b>0.871 ± 0.03</b>	6.64 ± 0.63	<b>0.633 ± 0.08</b>	<b>0.823 ± 0.06</b>

RMSE minimization is achieved through training, where the network adjusts its internal representations via gradient descent. In Fig. 3, we illustrate the training dynamics for  $K = 8$  under Configuration 1 on the PTC MR dataset. In this case, training yields an RMSE of  $4.087 \pm 0.395$ , with  $\tau = 0.624 \pm 0.071$  and  $\rho = 0.808 \pm 0.057$ . Notably, this corresponds to an RMSE improvement of approximately 28.30%.

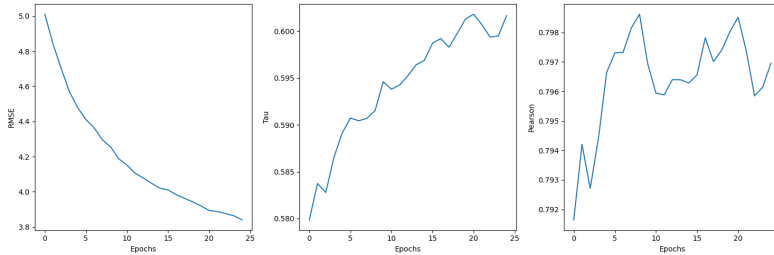


Figure 3: The training curves of U-GEDAN on the test-set of RMSE,  $\tau$  and  $\rho$  respectively.

An additional analysis can be performed by observing the scatter plot between the ground-truth GED and the predicted values across training epochs. Over the 25 training epochs, we observe the evolution in the model’s internal representations, which directly affects its predictions. In Fig. 4, we report the scatter plots at three stages of training: (a) epoch 1, (b) epoch 13, and (c) epoch 25. Each point represents a graph pair. The red arrow highlights a specific graph pair whose prediction significantly improves over time, moving closer to the identity line.

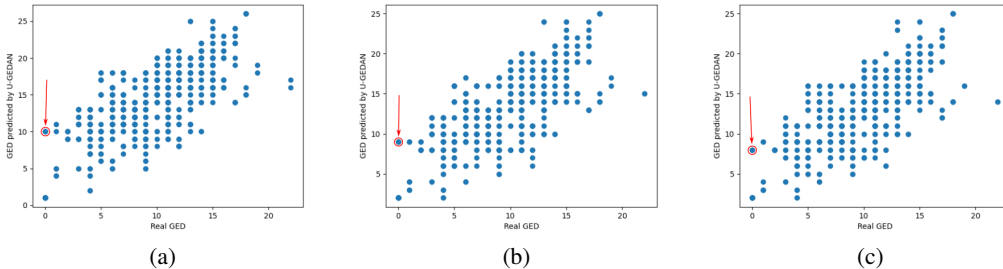


Figure 4: Scatter plots showing the GED predicted by U-GEDAN and ground-truth GED values at different training epochs: (a) epoch 1, (b) epoch 13, and (c) epoch 25.

The illustrative case, highlighted by the red arrow, is a graph pair with a very low ground-truth GED, initially predicted with a RMSE greater than 10. As training progresses, the predicted GED for this

graph pair gradually decreases, moving closer to the identity line. This behavior demonstrates the model’s ability to refine its internal representation over time.

This improvement is achieved in an unsupervised way, without direct supervision on the GED values, showing that U-GEDAN can internally structure representations that aligns with true graph distances.

## B Details of the GED Approximation

In this section, we report the results obtained for each configuration used in our GED approximation experiments. We selected three benchmark datasets [36]: AIDS, MUTAG, and PTC MR (see Table 4).

For computational feasibility, we restrict the graph sizes: only graphs with at most 9 nodes for AIDS, 16 nodes for MUTAG, and 10 nodes for PTC MR are included. This constraint is essential, as the precomputed labels used for training are based on GED values. Given that GED computation is NP-hard, these restrictions enable the generation of exact distances within a reasonable amount of time.

Table 4: Characteristics of the dataset used in the GED approximation.

AIDS [36]			MUTAG [36]			PTC MR [36]		
N. graph pairs	Avg. nodes	Avg. edges	N. graph pairs	Avg. nodes	Avg. edges	N. graph pairs	Avg. nodes	Avg. edges
190096	8.08	15.39	5776	13.29	28.08	16900	6.95	13.00

Furthermore, this setting allows us to build upon the recent analysis by Yang et al. [19], which highlights the potential to achieve high-quality GED approximations even in low-label regimes. In particular, we use the MUTAG dataset to explore how models behave under data scarcity conditions. Specifically, the number of graph pairs used in our experiments is as follows: MUTAG contains 5576 pairs, PTC MR contains 16900 pairs, and AIDS contains 190096 pairs.

We define five distinct cost configurations, summarized in Table 5, each modeling a different edit cost scenario for GED approximation.

1. The first configuration serves as a baseline, where all operations—node and edge insertions, deletions, and substitutions—have uniform costs set to 1, as commonly assumed in several models.
2. In the second configuration, the costs of inserting and deleting nodes are twice as expensive as the operations on edges.
3. In the third, edge insertions and deletions are assigned a cost twice as high as that of node operations.
4. In the fourth, insertions are twice as expensive as deletions.
5. In the fifth, deletions are twice as expensive as insertions.

Table 5: Operation costs of the datasets used in the GED approximation test.

Configurations	Type	Node Insertion Cost	Node Deletion Cost	Edge Insertion Cost	Edge Deletion Cost
Conf. 1	Baseline	1	1	1	1
Conf. 2	Symmetric	2	2	1	1
Conf. 3	Symmetric	1	1	2	2
Conf. 4	Asymmetric	2	1	2	1
Conf. 5	Asymmetric	1	2	1	2

### B.1 Results For Each Configuration

In Tab. 6, 7, 8, 9, 10, we present the results obtained from each model on the three datasets. All results are obtained by cross-validation with 5-fold K-fold scheme, using the 10% of training set as validation set for model selection. For each fold, we select the model with the best performance on the validation set and then use it for inference on the test set.

A comparative analysis of the results across configurations confirms the absence of a universally superior model, consistent with the no-free-lunch theorem [39].

Table 6: GED Approximation with Configuration 1.

MODEL	AIDS [36]			MUTAG [36]			PTC MR [36]		
	RMSE	$\tau$	$\rho$	RMSE	$\tau$	$\rho$	RMSE	$\tau$	$\rho$
SimGNN (2019) [15]	4.71 ± 0.36	<b>0.563 ± 0.04</b>	<b>0.793 ± 0.04</b>	14.20 ± 2.40	0.541 ± 0.07	0.798 ± 0.06	5.12 ± 0.40	<b>0.698 ± 0.05</b>	<b>0.881 ± 0.03</b>
GREED (2022) [16]	3.10 ± 0.20	0.349 ± 0.06	0.545 ± 0.06	5.66 ± 0.23	0.515 ± 0.07	0.705 ± 0.09	<b>2.18 ± 0.08</b>	0.666 ± 0.06	0.849 ± 0.04
ERIC (2022) [17]	6.30 ± 0.41	0.349 ± 0.06	0.545 ± 0.06	15.22 ± 2.78	0.512 ± 0.12	0.705 ± 0.09	5.83 ± 1.62	0.685 ± 0.05	0.871 ± 0.04
GraphEdX <sub>XOR</sub> (2024) [18]	4.26 ± 0.86	0.535 ± 0.07	0.730 ± 0.12	<b>5.47 ± 0.19</b>	0.593 ± 0.02	<b>0.861 ± 0.01</b>	3.38 ± 1.33	0.614 ± 0.16	0.784 ± 0.17
U-GEDAN	3.54 ± 0.14	0.437 ± 0.06	0.652 ± 0.06	13.30 ± 0.85	<b>0.611 ± 0.09</b>	0.852 ± 0.04	3.51 ± 0.31	0.649 ± 0.07	0.823 ± 0.05
S-GEDAN	<b>2.82 ± 0.19</b>	0.484 ± 0.05	0.694 ± 0.05	6.01 ± 0.66	0.608 ± 0.09	0.855 ± 0.04	3.18 ± 0.65	0.655 ± 0.08	0.826 ± 0.07

Table 7: GED Approximation with Configuration 2.

MODEL	AIDS [36]			MUTAG [36]			PTC MR [36]		
	RMSE	$\tau$	$\rho$	RMSE	$\tau$	$\rho$	RMSE	$\tau$	$\rho$
SimGNN (2019) [15]	6.00 ± 0.45	<b>0.583 ± 0.04</b>	<b>0.803 ± 0.03</b>	6.53 ± 1.19	<b>0.615 ± 0.05</b>	0.827 ± 0.05	4.93 ± 0.60	<b>0.775 ± 0.05</b>	<b>0.928 ± 0.03</b>
GREED (2022) [16]	<b>2.92 ± 0.09</b>	0.334 ± 0.07	0.571 ± 0.07	4.48 ± 0.86	0.585 ± 0.04	0.676 ± 0.06	<b>2.06 ± 0.18</b>	0.711 ± 0.05	0.881 ± 0.05
ERIC (2022) [17]	6.16 ± 0.48	0.575 ± 0.04	0.797 ± 0.03	6.02 ± 0.30	0.591 ± 0.06	<b>0.849 ± 0.02</b>	6.34 ± 1.29	0.762 ± 0.03	0.902 ± 0.03
GraphEdX <sub>XOR</sub> (2024) [18]	7.14 ± 0.14	0.537 ± 1.36	0.739 ± 0.06	4.08 ± 0.82	0.569 ± 0.11	0.725 ± 0.08	3.44 ± 1.79	0.671 ± 0.19	0.820 ± 0.18
U-GEDAN	3.91 ± 0.09	0.482 ± 0.06	0.698 ± 0.05	6.34 ± 0.80	0.595 ± 0.11	0.813 ± 0.05	3.44 ± 0.24	0.742 ± 0.05	0.897 ± 0.03
S-GEDAN	3.52 ± 0.14	0.511 ± 0.04	0.721 ± 0.04	<b>3.36 ± 0.49</b>	0.587 ± 0.09	0.829 ± 0.04	2.85 ± 0.47	0.770 ± 0.02	0.917 ± 0.02

Table 8: GED Approximation with Configuration 3.

MODEL	AIDS [36]			MUTAG [36]			PTC MR [36]		
	RMSE	$\tau$	$\rho$	RMSE	$\tau$	$\rho$	RMSE	$\tau$	$\rho$
SimGNN (2019) [15]	13.20 ± 3.83	0.497 ± 0.04	0.670 ± 0.06	10.72 ± 0.28	0.469 ± 0.04	0.618 ± 0.04	12.91 ± 1.24	0.579 ± 0.07	0.760 ± 0.07
GREED (2022) [16]	<b>3.05 ± 0.16</b>	0.467 ± 0.05	0.663 ± 0.06	4.96 ± 0.78	<b>0.592 ± 0.05</b>	0.659 ± 0.06	<b>2.85 ± 0.34</b>	<b>0.676 ± 0.07</b>	<b>0.847 ± 0.06</b>
ERIC (2022) [17]	12.24 ± 0.83	0.467 ± 0.05	0.663 ± 0.05	8.12 ± 0.59	0.573 ± 0.07	0.809 ± 0.03	13.13 ± 2.02	0.611 ± 0.05	0.787 ± 0.05
GraphEdX <sub>XOR</sub> (2024) [18]	10.76 ± 0.50	<b>0.586 ± 0.01</b>	<b>0.803 ± 0.02</b>	<b>4.07 ± 0.90</b>	0.551 ± 0.09	0.715 ± 0.11	5.39 ± 0.27	0.637 ± 0.02	0.815 ± 0.02
U-GEDAN	6.72 ± 0.18	0.398 ± 0.05	0.608 ± 0.04	15.12 ± 1.18	0.569 ± 0.08	<b>0.830 ± 0.03</b>	6.29 ± 0.40	0.639 ± 0.06	0.815 ± 0.05
S-GEDAN	5.88 ± 0.28	0.426 ± 0.05	0.641 ± 0.04	4.08 ± 0.56	0.582 ± 0.08	0.825 ± 0.04	5.42 ± 1.03	0.664 ± 0.07	0.835 ± 0.06

Table 9: GED Approximation with Configuration 4.

MODEL	AIDS [36]			MUTAG [36]			PTC MR [36]		
	RMSE	$\tau$	$\rho$	RMSE	$\tau$	$\rho$	RMSE	$\tau$	$\rho$
SimGNN (2019) [15]	9.55 ± 0.80	0.542 ± 0.05	0.770 ± 0.05	8.87 ± 0.81	<b>0.641 ± 0.02</b>	<b>0.848 ± 0.02</b>	10.57 ± .98	0.678 ± 0.04	0.850 ± 0.03
GREED (2022) [16]	<b>3.06 ± 0.22</b>	0.484 ± 0.07	0.698 ± 0.06	4.77 ± 0.67	0.596 ± 0.04	0.648 ± 0.04	<b>3.25 ± 0.19</b>	<b>0.696 ± 0.05</b>	<b>0.858 ± 0.03</b>
ERIC (2022) [17]	10.90 ± 0.69	0.507 ± 0.05	0.725 ± 0.05	9.29 ± 0.60	0.413 ± 0.07	0.596 ± 0.05	11.02 ± 1.47	0.613 ± 0.08	0.779 ± 0.09
GraphEdX <sub>XOR</sub> (2024) [18]	8.56 ± 0.28	<b>0.596 ± 0.03</b>	<b>0.827 ± 0.01</b>	<b>4.50 ± 0.61</b>	0.610 ± 0.04	0.816 ± 0.05	5.16 ± 0.48	0.664 ± 0.04	0.844 ± 0.04
U-GEDAN	5.77 ± 0.12	0.432 ± 0.04	0.675 ± 0.04	7.50 ± 0.72	0.604 ± 0.10	0.827 ± 0.06	5.75 ± 0.52	0.638 ± 0.06	0.831 ± 0.04
S-GEDAN	5.17 ± 0.26	0.479 ± 0.04	0.718 ± 0.04	4.82 ± 0.58	0.599 ± 0.10	0.825 ± 0.06	5.27 ± 1.04	0.681 ± 0.08	0.856 ± 0.06

Table 10: GED Approximation with Configuration 5.

MODEL	AIDS [36]			MUTAG [36]			PTC MR [36]		
	RMSE	$\tau$	$\rho$	RMSE	$\tau$	$\rho$	RMSE	$\tau$	$\rho$
SimGNN (2019) [15]	10.14 ± 0.72	<b>0.562 ± 0.04</b>	0.763 ± 0.04	7.96 ± 1.38	<b>0.642 ± 0.05</b>	<b>0.840 ± 0.05</b>	9.32 ± 0.68	0.717 ± 0.05	<b>0.890 ± 0.03</b>
GREED (2022) [16]	<b>3.14 ± 0.22</b>	0.509 ± 0.06	0.690 ± 0.07	<b>4.51 ± 0.40</b>	0.630 ± 0.03	0.697 ± 0.04	<b>2.99 ± 0.46</b>	<b>0.719 ± 0.07</b>	0.872 ± 0.05
ERIC (2022) [17]	11.80 ± 0.33	0.461 ± 0.04	0.622 ± 0.04	9.76 ± 1.27	0.560 ± 0.05	0.779 ± 0.02	11.69 ± 1.37	0.652 ± 0.08	0.769 ± 0.09
GraphEdX <sub>XOR</sub> (2024) [18]	9.56 ± 0.25	0.545 ± 0.01	<b>0.832 ± 0.02</b>	4.92 ± 0.85	0.529 ± 0.06	0.688 ± 0.07	4.64 ± 0.25	0.712 ± 0.02	0.879 ± 0.01
U-GEDAN	6.00 ± 0.10	0.433 ± 0.04	0.658 ± 0.04	8.65 ± 0.94	0.513 ± 0.05	0.741 ± 0.02	5.56 ± 0.55	0.650 ± 0.06	0.839 ± 0.05
S-GEDAN	5.50 ± 0.25	0.486 ± 0.04	0.705 ± 0.04	4.91 ± 0.47	0.521 ± 0.06	0.755 ± 0.03	5.51 ± 1.10	0.693 ± 0.06	0.848 ± 0.07

## C Details of Edit Cost Optimization

For edit cost optimization we use 3 molecular datasets, varying the size and type of task required. The graphs are limited to 32 nodes, thus using the Gumbel-Sinkhorn 64x64 module, with the performance reported in Appendix E. We show the characteristics of the datasets used in Table 11.

Table 11: Characteristics of the dataset used in edit cost optimization.

FreeSolv [40]			BBBP [41]			ZINC [42]		
N. graphs	Avg. nodes	Avg. edges	N. graphs	Avg. nodes	Avg. edges	N. graphs	Avg. nodes	Avg. edges
642	8.72	16.78	1734	20.84	44.88	9615	22.78	48.91

FreeSolv [40] is a small dataset that collects hydration free energies (HFE), both experimental and calculated, for small molecules in water. It is commonly used for the prediction of molecular properties in the field of computational chemistry. The choice of this dataset is due to its small size, especially in application contexts one does not have a lot of data, so we verified that the model would work in this context.

BBBP (Blood-Brain Barrier Penetration) [41] is dataset that models the permeability of the blood-brain barrier, which can prevent the passage of the of drugs, hormones and neurotransmitters. The dataset tests the ability of a molecule to cross this barrier with binary labels. The dataset is not large to test the model in a real scenario of experimental data, where there are often not many.

ZINC [42] is a large dataset of molecules, primarily used for virtual screening in drug discovery. The ZINC database contains millions of chemical compounds with information on their physicochemical properties, molecular structures, and commercial availability. We used a reduced version by testing the scalability of our model on a more complex feature.

### C.1 Loss and Training Strategy

The training of the model S-GEDAN is based on the joint optimization of two loss functions:

- a contrastive loss based on the softmax applied to GED ,
- and a loss for the downstream task (e.g., regression or classification).

During training, for each query we select  $H$  keys from the training set by causal sampling, ensuring semantic consistency with the target to be predicted. Of these  $H$  keys, the first and last are fixed while the remaining  $H - 2$  are selected according to the nature of the task.

In detail:

- For regression, the fixed keys correspond to the instances with minimum and maximum target value; the middle keys are selected so that their targets are ordered with respect to that of the query.
- For binary classification,  $(H - 2)/2$  instances are selected for each class. The two fixed keys represent one instance of the negative class and one instance of the positive class.

This strategy ensures a balanced and semantically consistent distribution, although it does not include hard negative sampling, which may make optimization less effective in ambiguous cases. The introduction of more sophisticated sampling techniques is left for future work.

Contrastive loss, applied to GED distances, is defined as:

$$\mathcal{L}_i^{\text{contr}} = -\log \left( \frac{\exp(-\text{GED}_{i,y_i}/T)}{\sum_{j=1}^H \exp(-\text{GED}_{i,j}/T)} \right) \quad (20)$$

where:

- $\text{GED}_{i,j}$  is the distance between the query  $i$  and the key  $j$ ,
- $y_i \in \{1, \dots, H\}$  is the index of the positive key,
- $T \in \mathbb{R}^+$  is the temperature hyperparameter of the softmax distribution.

This formulation can be interpreted as a differentiable approximation of minimizing the distance between the query and its assigned positive key, while simultaneously penalizing the negative keys proportionally to their similarity (i.e., inverse of GED). As a result, the learned distribution encourages alignment with semantically coherent keys and drives the model to build discriminative representations.

The assignment of the positive key  $y_i$  depends on the nature of the task:

- For regression, the positive key is the one with the closest label value to the query value, i.e.:

$$y_i = \arg \min_j |y_i^{\text{true}} - y_j^{\text{key}}| \quad (21)$$

ensuring that the model focuses on neighboring keys in the continuous target domain.

- For classification, a key belonging to the same class as the query is selected. In the presence of multiple candidate keys with the same class, the average GED distance of multiple candidate keys to the query is selected. This approach promotes a more robust semantic match, avoiding outliers.

The loss associated with the downstream task is computed using a separate MLP that takes as input the set of  $\text{GED}_{i,j}$  values. Since semantic coherence between the query and keys has been preserved through the sampling strategy, we can directly optimize with respect to the query’s label as follows:

- For the regression:

$$\mathcal{L}_i^{\text{reg}} = \|\hat{y}_i - y_i^{\text{true}}\|^2 \quad (22)$$

- For binary classification:

$$\mathcal{L}_i^{\text{cls}} = -y_i^{\text{true}} \log \hat{y}_i - (1 - y_i^{\text{true}}) \log(1 - \hat{y}_i) \quad (23)$$

Finally, the total loss is obtained as a weighted combination of the two components:

$$\mathcal{L} = \frac{1}{B} \sum_{i=1}^B (\mathcal{L}_i^{\text{contr}} + \lambda \cdot \mathcal{L}_i^{\text{task}}) \quad (24)$$

where:

- $B$  is the batch size,
- $\mathcal{L}_i^{\text{task}} \in \{\mathcal{L}_i^{\text{reg}}, \mathcal{L}_i^{\text{cls}}\}$  depending on the task,
- $\lambda \in \mathbb{R}^+$  It is a hyperparameter that balances the two components.

## C.2 Edit Cost Optimization Effect

In Fig. 5, 6, 7, we present the *Principal Components Analysis* (PCA) [53] obtained on the FreeSolv [40], BBBP [41] and ZINC [42] datasets, respectively. PCA is performed on the 16 GED embedding values predicted by the networks repeating the process 3 different samplings (identify by letter (a), (b), (c) in the respectively figures). We present on the left the baseline version (U-GEDAN), in which the edit cost operations are uniform, on the right, the version optimized (S-GEDAN).

Each dot represents a graph while the color indicates the value of the associated label. As can be easily observed, PCA highlights the effect of optimization on the GED produced. The optimized methods show, in general, a better gradient transition, resulting in a more accurate alignment of target values.

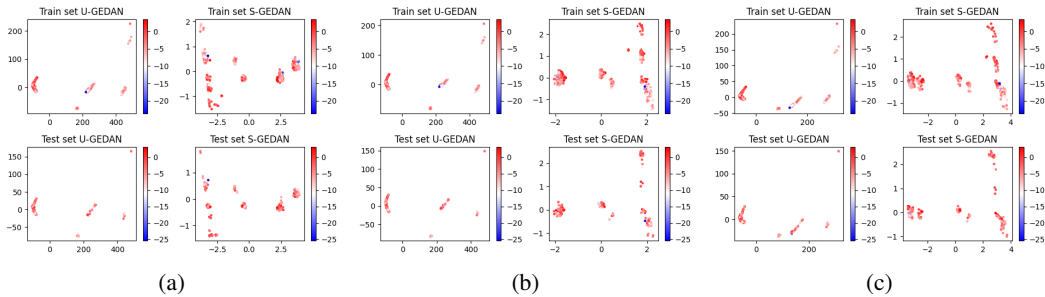


Figure 5: PCA of the FreeSolv dataset [40].

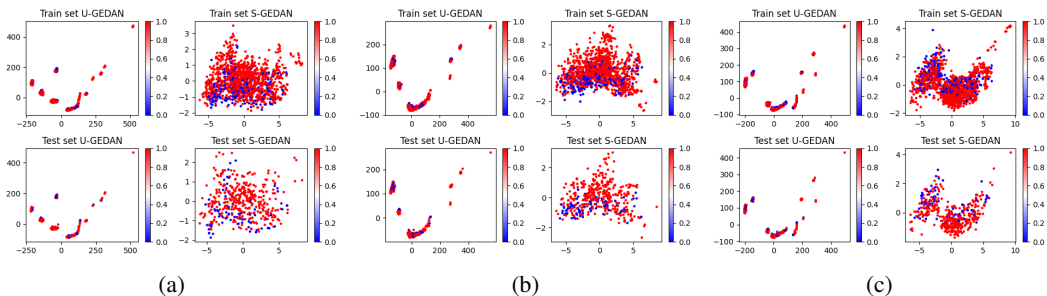


Figure 6: PCA of the BBBP dataset [41].

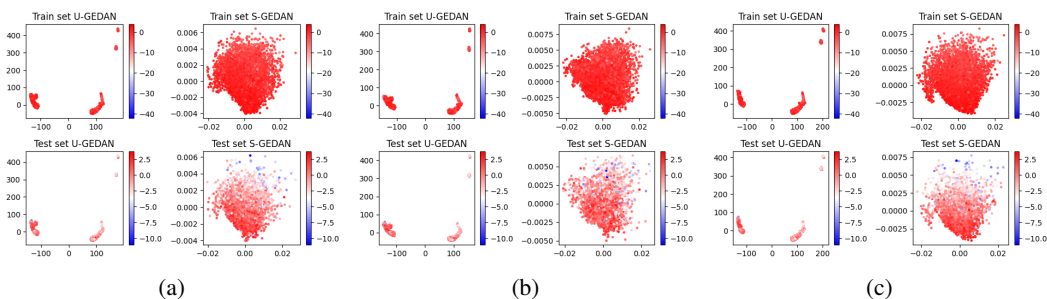


Figure 7: PCA of the ZINC dataset [42].

## D Inference Time Analysis

As discussed in the main paper, one of the limitations of our model lies in its higher resource usage, which makes it slower and less optimized compared to state-of-the-art methods. In this section, we provide a detailed analysis of the model’s inference time. All inference tests are conducted on a single GeForce RTX 4070 Ti GPU with a batch size of 64.

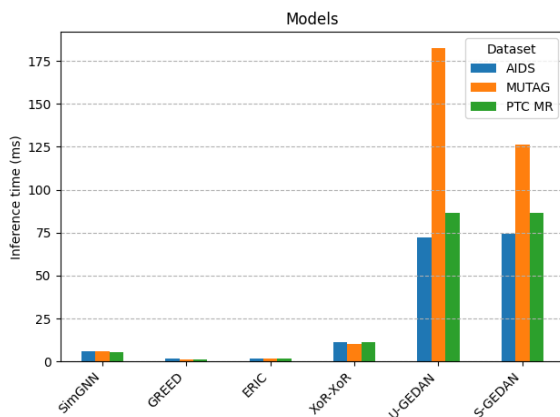


Figure 8: Time comparison in milliseconds of models inference on GED approximation dataset.

As shown in Fig.8, our model is significantly slower than the benchmarks. This slowdown is primarily due to an overhead introduced by matrix initialization rather than the number of trainable parameters.

Table 12 reports the average number of trainable parameters for each model. Our U-GEDAN model has fewer parameters than ERIC [17], while S-GEDAN has fewer parameters than GREED [16].

Nevertheless, GEDAN models are slower in practice. Notably, models such as SimGNN [15] and GraphEdX [18] achieve excellent performance with a very small parameter count.

Table 12: Average trainable parameters used to approximate the GED

SimGNN (2019) [15]	GREED (2022) [16]	ERIC (2022) [17]	GraphEdX (2024) [18]	U-GEDAN (Our)	S-GEDAN (Our)
9249	151553	29157	5785	15306	53182

As mentioned above in the section on limitations, the main bottleneck lies in matrix management. Despite the use of optimized operations such as broadcasting, this component remains the most time-consuming part of the computation.

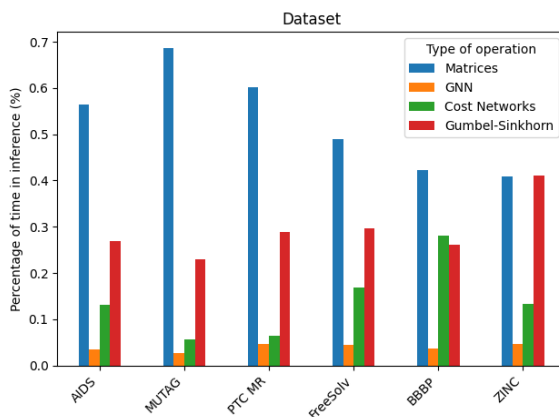


Figure 9: Time comparison of GEDAN’s components on inference.

As shown in Fig. 9, matrix operations account for approximately 40% to 70% of the total inference time. The Gumbel-Sinkhorn network constitutes the next most significant contribution, while both the GNN operations and the edit cost computation have a comparatively minor impact.

Inference time for molecular prediction is also compared against GraphMaskExplainer [46]. Both GEDAN and the reference GNN have 4 layers to ensure that prediction time is not biased by depth. In the direct comparison, first column of Fig.2 (a), only GEDAN’s result is reported, as GraphMaskExplainer cannot be applied in this case. The other two columns refer to predictions shown in Fig.2 (b) and (c), where GEDAN is faster.

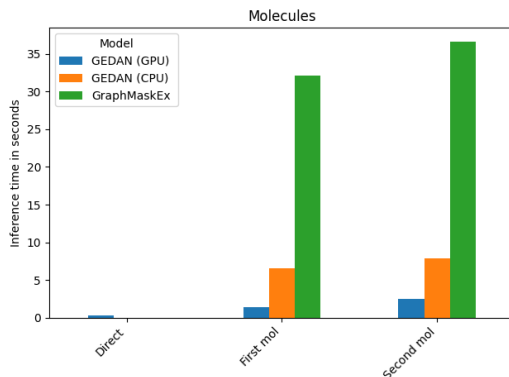


Figure 10: Time comparison in seconds of prediction of GEDAN molecules compared with GNN analyzed by GraphMaskExplainer [46].

## E Model Details

To implement the proposed method, some preprocessing operations need to be performed on the data. The method requires bipartite graphs, which results in the use of square matrices. To fulfil this constraint, additional nodes with dummy representation are added to each graph.

In addition to these structural nodes, additional padding nodes are introduced to ensure that the matrices not only remain square, but also reach a pre-defined size (e.g.  $64 \times 64$  or  $128 \times 128$ ). These padding nodes also have a dummy representation, used exclusively to adjust the size of the matrix.

To manage this structure, binary masks that selectively obscure certain pairs of nodes are computed and applied. However, this strategy is not an optimal solution, both because of the increase in memory space required and the introduction of computationally unnecessary computations. Improvements in this regard are in future work.

### E.1 Gumbel-Sinkhorn

To obtain a good  $\mathbf{P}$ , we modify the version of the original Gumbel-Sinkhorn network [24, 54], using the Truncated Gumbel [55] to reduce the gradient variance and add stability. We then sample with the Gumbel-Max Trick [56] while maintaining differentiability. Finally we stabilize the normalization of Sinkhorn [57] with an early stop, improving efficiency and limiting gradient vanishing [58].

The Gumbel-Sinkhorn network has been trained for 200 epochs on matrices of sizes  $32 \times 32$ ,  $64 \times 64$  and  $128 \times 128$ . The matrices used for training are randomly generated, with 250000 samples for each of the three dimensions. For each matrix, *Linear Sum Assignment* (LSA) is calculated and used as a reference label. Optimization is performed by minimizing the Huber Loss, with a learning rate of 0.001 and using the Adam optimizer. Training also includes a curriculum learning phase, during which many matrices with zero values on the diagonal are initially proposed, a strategy that facilitated model convergence. In addition, an early stopping mechanism is applied on the Sinkhorn process, with a limit of 50 iterations, where the stopping condition is determined by a difference between consecutive iterations of less than  $1e-4$ .

To test the performance of the Gumbel-Sinkhorn network, 10000 new random matrices are generated, for which the LSA varies between 0.001 and 199.750, with an average of 77.375. The overall performance of the model calculated on the  $64 \times 64$  matrices using high temperatures has a  $\tau$  value of 0.991, a  $R^2$  coefficient of 0.993 and a *Root Mean Square Error* (RMSE) of 3.940. These configurations are kept stable in the pre-trained versions in the U-GEDAN and S-GEDAN models.

### E.2 U-GEDAN and S-GEDAN

GIN layers are implemented using a simple MLP, followed by a ReLU activation function to introduce non-linearity. The output of each layer is then normalized using LayerNorm. Before calculating distances, the embedding vectors are normalized, resulting in representations on a unit sphere (spherical embeddings).

As for the functions  $f^{(k)}$ , we concatenate the representations of the two nodes involved and provide the result as input to an MLP. This MLP employs a ReLU as an intermediate activation function and applies a softplus function with parameter  $\beta = 5$  on the final output, as described in the main body of the text.

We use the Adam optimizer. The learning rate, number of layers  $K$ , embedding size, and batch size are chosen according to the dataset and type of model considered. We explored several configurations, and in the main paper we use those that offer the best trade-off between accuracy and computational cost.

For U-GEDAN and S-GEDAN training of the GED approximation we use a NVIDIA A100. Cost optimization training is performed on a cluster using two NVIDIA H100s. The model implementation is carried out using PyTorch (version 2.2.0) and the PyTorch Geometric library (version 2.4.0). Hardware acceleration is enabled via CUDA (version 12.1). The source code for the model is publicly available at <https://github.com/GEDAN-neurips2025/GEDAN>.

## F Predicted Molecules

In the main paper, we present two representative molecules along with their predictions, highlighting how our model is able to perform both direct comparisons between molecules and consistent analyses of their overall chemical behavior.

Here, we extend this analysis by presenting additional molecular examples to further illustrate these capabilities. Specifically, we study direct molecular comparisons, symmetry-based reasoning, and maintenance of chemical consistency over a larger and more structurally complex set of molecules. These examples serve to demonstrate the robustness and generalizability of our approach, which goes beyond the molecules shown in the main paper.

### F.1 Direct Comparison

To assess the model's ability to make fine-grained chemical reasoning, we consider pairs of structurally similar molecules with slight variations. These comparisons test whether the model is able to detect and reflect small but chemically significant differences in its predictions. As shown in Fig. 11, the model responds consistently to local changes, capturing many of the expected trends.

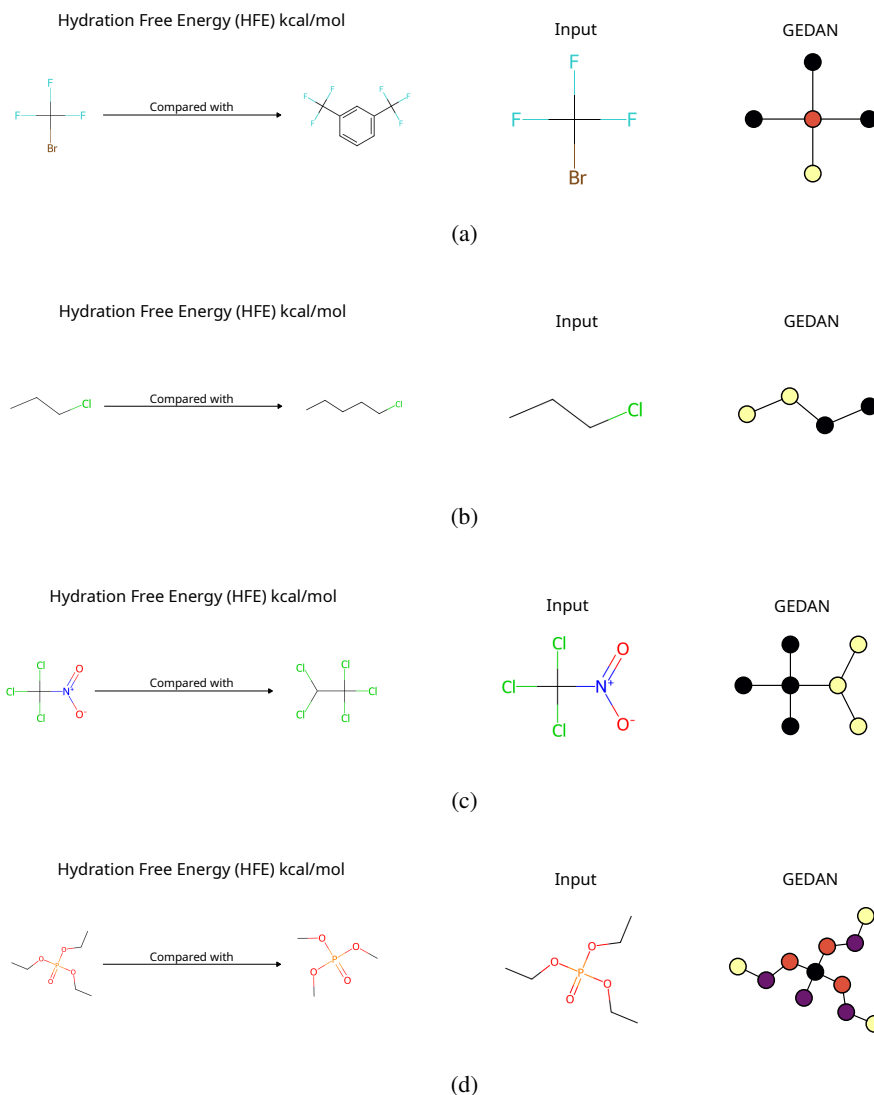


Figure 11: Direct comparison between pairs of similar molecules. Each panel (a–c) shows two molecules differing by a small chemical modification.

## F.2 Symmetric Molecules

Molecular symmetry poses a unique challenge for predictive models because it requires invariance or equivariance with respect to permutations of atoms or substructures. In this section, we evaluate the model’s ability to produce predictions that respect molecular symmetry, both at the level of global structure and local atoms. The examples in Fig. 12 demonstrate that our model maintains more symmetric predictions than GraphMaskExplainer [46].

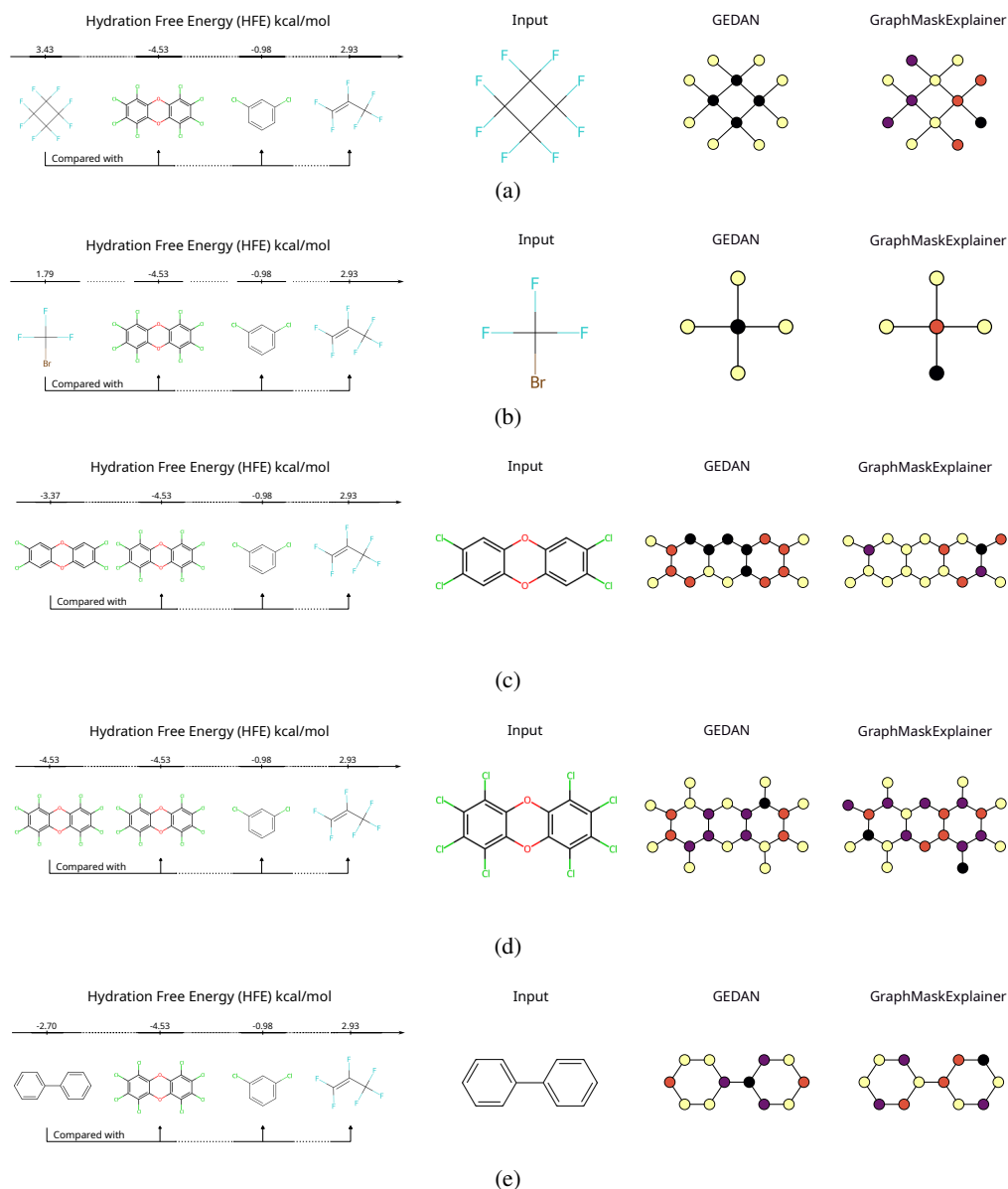


Figure 12: Model predictions on symmetric molecules. Each panel (a – e) illustrates the model’s ability to produce equivalent results for symmetrically equivalent atoms or substructures.

## F.3 Chemically Consistent Molecules

To assess the model’s ability to generalize to structurally different but chemically similar compounds, we evaluate its predictions on a set of molecules that share some functional properties. This analysis complements the main examples by demonstrating that the model preserves chemically meaningful

behavior beyond simple or symmetric cases. As shown in Fig. 13, the model produces consistent results.

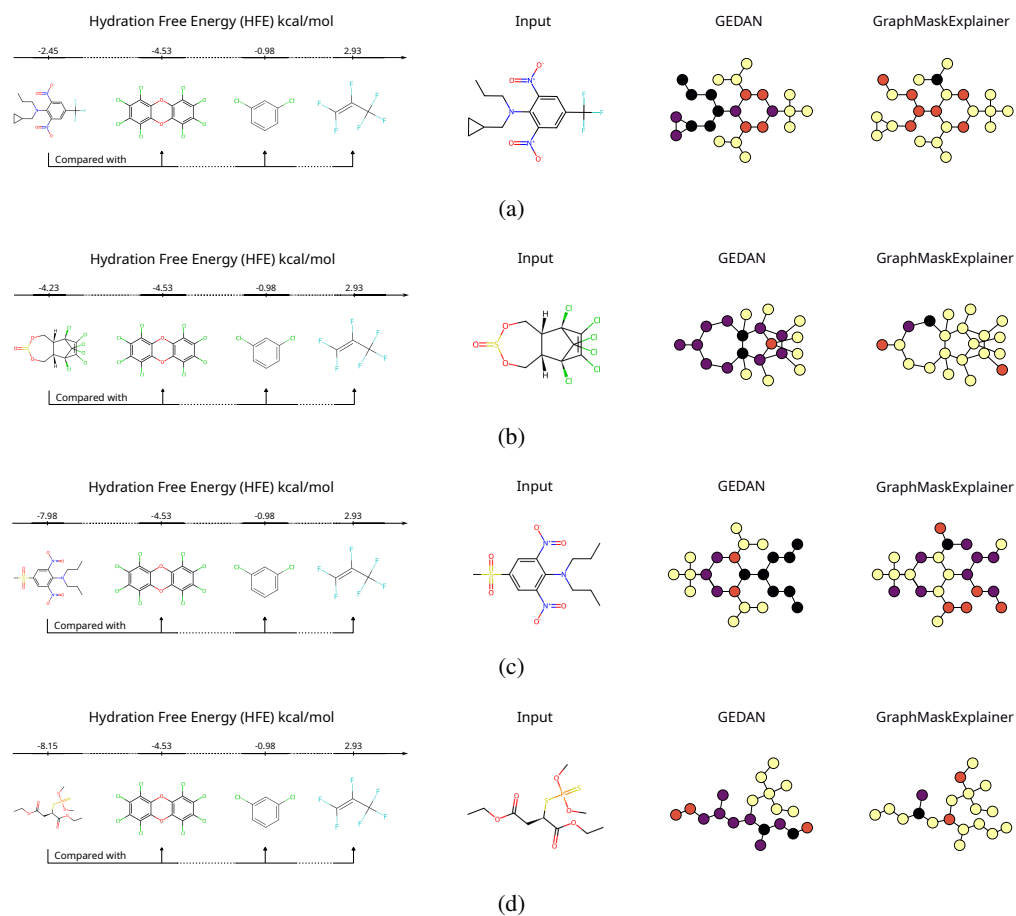


Figure 13: Predicted behavior on chemically consistent molecules. Each panel (a – d) shows a distinct molecule with structurally different motifs but similar chemical properties.